NREL/TP-451-5265 • UC Category: 271 • DE93000051

In-Situ Characterization of Growth and Interfaces in a-Si:H Devices

Annual Subcontract Report 1 May 1991 – 30 April 1992

NREL/TP--451-5265

DE93 000051

R. W. Collins, C. R. Wronski, I. An, Y. Li
Pennsylvania State University
University Park, Pennsylvania

NREL technical monitor: B. von Roedern

National Renewable Energy Laboratory
1617 Cole Boulevard
Golden, Colorado 80401-3393
A Division of Midwest Research Institute
Operated for the U.S. Department of Energy
under Contract No. DE-AC02-83CH10093

Prepared under Subcontract No. XG-1-10063-10

December 1992

NOTICE

Printed in the United States of America
Available from:
National Technical Information Service
U.S. Department of Commerce
5285 Port Royal Road
Springfield, VA 22161

Price: Microfiche A01
Printed Copy A04

Codes are used for pricing all publications. The code is determined by the number of pages in the publication. Information pertaining to the pricing codes can be found in the current issue of the following publications which are generally available in most libraries: *Energy Research Abstracts (ERA)*; *Government Reports Announcements* and Index (*GRA* and I); *Scientific and Technical Abstract Reports (STAR)*; and publication NTIS-PR-360 available from NTIS at the above address.

EXECUTIVE SUMMARY

Here the major conclusions of this research are enumerated.

(1) **The chemical potential of H in optimum plasma-enhanced CVD (PECVD) a-Si:H can be raised in a controllable fashion by exposure to atomic H generated by a heated filament.** If performed at the deposition temperature (~250°C) under specified conditions of filament power and H_2 pressure, irreversible conversion of ~$2x10^{21}$ cm^{-3} Si-Si bonds to Si-H bonds (4 at.% additional H) is possible to a depth of 200 Å or more, with minimal damage or etching. The process of H incorporation, studied optically in real time, exhibits reaction-limited (i.e. deep H trap-limited) kinetic behavior [see (3), below] throughout the optical penetration depth, i.e. the top 500 Å of the film. *See Sects. 3.1 and 3.11.*

(2) **Optical ellipsometry in the near uv is a sensitive probe of the conversion of Si-Si to Si-H bonds. As a result, the first real time studies of H-diffusion/trapping in the near surface region of the film have been performed.** In this study, we have determined the spectroscopic characteristics of Si-H bonds in the near uv. From this information we can use spectroscopic ellipsometry (SE) in real time to characterize the volume fraction of material converted in the process of H-treatment. We find that roughly 4 vol.% conversion occurs for every 1 at.% H incorporated. This ratio suggests that the fundamental unit of electronic polarizability is not the single Si-H bond, but rather a larger unit such as an $Si\text{-}Si_3H$ (Si-centered) tetrahedron. We detect the volume occupied by such units versus time. *See Sect. 3.2.*

(3) **The optically-detectable conversion of Si-Si bonds to Si-H bonds exhibits kinetics limited by H deep-trapping [i.e. $f_{Si\text{-}H}=f_0\{1-\exp(-\alpha t)\}$], in the top 500 Å of the film.** This also implies that the diffusive configurations (free or shallow-trapped H) are undetectable in the optical measurement. The lack of sensitivity to the diffusive H may imply a high diffusion coefficient and/or low concentration for the configurations. Based on the distribution of rate coefficients, there appear to be two diffusion/reaction mechanisms occurring. The rate coefficients (α) associated with the two mechanisms differ by one order of magnitude. In optimum PECVD a-Si:H, upon equilibration at 250°C, we find that ~ten bonds associated with the slow mechanism are broken for every one bond associated with the fast mechanism. The appearance of the fast mechanism correlates with voids in the film, and may result from faster H-diffusion through void channels and thus a higher capture rate of diffusive H by traps. The dominant rate coefficient is constant with temperature within confidence limits, suggesting that H-deep trapping occurs via direct capture with no energy barrier, e.g. due to configurational change. *See Sect. 3.4.*

(4) **The near-surface diffusion coefficient of H (D_H) in our situation must be at least 2-3 orders of magnitude higher than that measured in the conventional manner with a-Si:H/a-Si:H:D multilayers.** This conclusion is necessitated by the observation of the reaction- (rather than diffusion-) limited kinetic behavior [see (3)] for the conversion of Si-Si bonds to Si-H bonds to a depth of 500 Å. The origin of the apparent discrepancy is that in our measurements the H atoms are injected into the transport level at the surface, and a difference in the chemical potential drives the H-diffusion. This is an important realization because the latter phenomena presumably occur during the growth of a-Si:H. Thus, the conventionally-determined D_H is not relevant for the interaction of H with the growing film. *See Sect. 3.5.*

(5) **A surface oxide layer on a-Si:H of a few monolayers thickness is an extremely effective diffusion barrier for H, and prevents equilibration of gas phase and thin film chemical potentials.** This suggests that the diffusion process begins with a H atom bonded on the a-Si:H surface. From there, a bond-switching mechanism may result in subsurface penetration. When the surface is covered with stronger Si-O bonds, this mechanism is blocked. For this reason, all studies of H-diffusion from the gas phase must be performed in situ. *See Sect. 3.7.*

(6) **By monitoring the reconversion of Si-H bonds to Si-Si bonds upon terminating the H treatment after saturation, the kinetics of release of H from traps can be monitored, typically for traps located 1.3 to 1.9 eV below the H transport level at 250°C.** By far the majority of the traps that provide the optical signature of Si-H bonding are deep (i.e. >1.9 eV below the average transport level) and are not released over the period of one day even at 250°C. *See Sect. 3.8.*

(7) **If the chemical potential in the near surface region of the a-Si:H film is raised above a critical level in the H-treatment process, etching is observed.** Under etching conditions the near surface material is a relatively dense highly-ordered crystalline Si as thick as 15 Å. *See Sect. 3.9.*

(8) **Sputtered a-Si exhibits all the same basic phenomena as optimum PECVD a-Si:H, including reaction-limited behavior of Si-Si bond conversion, as well as the oxide barrier effect.** The main difference between PECVD a-Si:H and sputtered a-Si is the transient response of the Si-Si bond breaking upon H-treatment. In sputtered a-Si also, there appear to be two rate coefficients [see (3)] differing by an order of magnitude. However in sputtered a-Si, ~three bonds associated with the slow mechanism are broken for every one bond associated with the fast mechanism. The latter mechanism is attributed to more rapid diffusion through void channels that are more extensive in the sputtered samples of our study. *See Sect. 3.10.*

(9) **In the H-treatment process no additional dangling bonds are created even though ~$2x10^{21}$ cm^{-3} Si-Si bonds are broken.** Up to about 4 at.% extra bonded H can be incorporated into the network (80% of which is associated with the 2000 cm^{-1} monohydride ir absorption band) with the filament H-treatment. For films with high incorporated H-content prepared with high power filament treatments, the band tail state distribution is nearly unchanged (~50 meV Urbach parameter), and the initial kinetics of the Staebler-Wronski (SW) Effect also remain unchanged from those of untreated materials. For films with lower incorporated H content (~1-2 at.%) prepared with low power filament treatments, a ~40% improvement in the defect density in the fully light-soaked state has been achieved in comparison to similarly-prepared untreated films. We conclude that the H-treatment process shows promise in improving a-Si:H stability, however, further optimization and understanding of the process is required. *See Sect. 3.11.*

(10) **A clear connection is observed between film precursor surface diffusion length during growth and the ultimate properties of the bulk a-Si:H.** In particular, a surface smoothening process is detected by real time SE in the initial stages of growth once the first bulk density a-Si:H monolayer has formed. This represents the coalescence of nucleation-generated morphology through capillarity-driven surface diffusion. A suppression of the smoothening process is expected under low diffusion length growth conditions, and this behavior is verified experimentally under conditions of high power, and low and high substrate temperature, conditions known to lead to electronically defective material. *See Sect. 4.*

Table of Contents

1. Introduction

The growth of hydrogenated amorphous silicon (a-Si:H) by plasma enhanced chemical vapor deposition (PECVD) is an exceedingly complex process that involves many gas phase and solid surface chemical and physical processes, influenced by charged particle bombardment, uv light exposure etc. The following generic reaction pathways represent the types of processes that connect gas phase, surface, and sub-surface phenomena to the electronic properties [1]:

$$SiH_3(g) + Si_3Si(s)- \;<->\; Si_3Si\text{-}Si\text{-}H(s) + H_2(g) \qquad (1)$$

$$Si\text{-}H + Si\text{-}Si \;<->\; D^0 + Si\text{-}H\text{-}Si \qquad (2)$$

$$Si\text{-}H\text{-}Si + Si\text{-}Si(wk) \;<->\; Si\text{-}Si(sg) + Si\text{-}H\text{-}Si \qquad (3)$$

$$H(g) + Si\text{-}Si(s) \;<->\; Si\text{-}H\text{-}Si(s) \qquad (4)$$

Pathway (1) is based on experimental results that suggest SiH_3 is the predominant film precursor in low power (undepleted) rf discharges [2]. This is basically the second step of a process that first involves H extraction from the surface (e.g. by H or SiH_3), leaving a free bond for the attachment of the SiH_3 radical.

Reaction (2) is a subsurface reaction that generates a neutral defect. It has been proposed that the forward rate for (2) is enhanced under illumination [3], giving rise to the light induced dangling bond defects, D^0's, that characterize the Staebler-Wronski effect [4]. The general notation "Si-H-Si" represents the insertion of H at a Si-Si bond, which may (i) stabilize at that site in the bridging or bond-centered configuration, (ii) react to form an Si-H and D^0 at that site, or (iii) diffuse to another Si-Si bond position. In the specific case of reaction (2), the H may also diffuse back to its original dangling bond site. Reaction (3) represents relaxation of the network, whereby H diffuses through Si-Si bonds and stabilizes weaker (wk) Si-Si bonds in preference to stronger (sg) ones. Reaction (4) represents the insertion of atomic H from the gas phase into a Si-Si bond. Although more recent studies suggest the importance of the association of H into complexes [5], such as the H_2*, consisting of a bond center H and tetrahedral interstitial H [6], the simplified reactions (1)-(4) will suffice for the present discussion which motivates our work.

Much recent interest has been generated by altering gas phase and near-surface conditions to move the equilibrium points in the near-surface and subsurface reactions (2)-(4). For example, the generation of excess atomic H in the gas phase during growth drives reaction (4) in the forward direction, this, in turn, drives reaction (3) to stabilize the network. If the H-source is

removed, excess H in shallow traps leaves the network via reaction (4) in the reverse direction. Some authors have termed this process "chemical annealing", meaning that a chemical equilibrium is established during growth whereby only enough H is incorporated to terminate dangling bonds and relax strain [7].

In a more rigorous view of this process, one assumes that by increasing the concentration of atomic H in the gas phase, its chemical potential is increased [8]. Thus, H diffuses into the film by reaction (4) so as to equilibrate the gas phase and solid film chemical potentials. In doing so the chemical potential μ_H in the film moves to an energy in the tail of the weak Si-Si bond distribution via reaction (3). As a result, weak Si-Si bonds at or below μ_H are converted to Si-H bonds in order to minimize the Si-Si and Si-H bond "density-of-states" distribution at bond energies corresponding to μ_H. This results in an increase in order in the film over that which would be achieved in the absence of the excess H. If the atomic H is removed, i.e. at the end of deposition, free H in the transport path and in shallow traps may diffuse out from the film, but an elevated chemical potential remains in the film upon cooling, owing to the kinetic limitations associated with emptying the deep traps.

An increase in the thin film chemical potential through excess atomic H during growth will occur only if the rate of H diffusion into the film exceeds the growth rate. Otherwise equilibration itself is kinetically limited [1,8]. Kinetic limitations occur when the subsurface zone of thickness $L=D_H/R$ is reduced to a monolayer or less. In fact, if one were to use the diffusion coefficient D_H obtained from hydrogenated/deuterated multilayers, $2x10^{-16}$ cm^2/s (conservatively chosen to account for the effect of dispersion [9]), and the growth rate, R, of 2 Å/s typical of that used in conventional PECVD, then one would find that L~1 Å, meaning that our "optimum" PECVD process borders the kinetically-limited regime. At first sight it might suggest that material improvements can be made through further equilibration; however, our confidence in such an assessment is tempered by a lack of information on hydrogen diffusion processes in the growth environment.

Our research consists of two broad components. The first and by far the major component involves preparing a-Si:H by "optimum" PECVD, and exposing the final film to atomic hydrogen in situ at the growth temperature. The spirit of the research is very similar to that described in the previous paragraphs. The role of the gas phase atomic hydrogen is to raise the H chemical potential in the film above that which was established kinetically in the SiH_4 preparation plasma.

The processes of H-diffusion and incorporation in the exposed film are studied in real time by spectroscopic ellipsometry (SE); we obtain a dynamic picture of the processes by which the chemical potential in the film equilibrates with that in the gas phase. SE is sensitive to these phenomena through the packing density of Si-Si bonds whose polarizability gives rise to the broad peak in ε_2 near 3.75 eV. Because of the surface sensitivity of SE, ultrathin films can be

used if needed to ensure equilibration throughout the film thickness. Furthermore, SE is extremely sensitive to surface roughness thickness and bulk film thickness at submonolayer levels. Thus, we can ensure that the chemical potential in the gas phase is not increased to such a level that would result in significant etching and/or reordering of the surface atoms. In the literature, there is a relative lack of information on H diffusion in a-Si:H under conditions of film growth. To our knowledge no real time measurements of such processes have been undertaken.

The properties of films prepared by alternating "optimum" PECVD growth of a thin film and H-exposure to ensure equilibration of the chemical potential throughout the film have been studied. There are two unique aspects to our approach. First, we use atomic hydrogen exposures generated by a filament heated to ~2000 K. Our experience with diamond film growth has suggested that this is a very effective and controllable method of raising the gas phase H chemical potential. Furthermore, with the filament approach there are no other effects such as ion bombardment, uv light exposure etc., associated with various direct plasma treatments. Second, the real time ellipsometric probe allows us to converge onto the proper conditions of hydrogenation (e.g. filament power) that allow a maximum chemical potential, and thus maximum ordering in the film, *with no significant etching on the time scale of the experiment.* Finally, the heated filament approach is vastly less expensive than some H-treatment alternatives (i.e. ECR) and can be performed with the sample mounted in the standard PECVD configuration.

The second broad component of our research will only be discussed briefly in this report as it was a outgrowth of our previous work on single wavelength ellipsometry [10]. With the new real time spectroscopic capability developed at Penn State, we are now in a position to quantify the nucleation and growth process at an unprecedented level. We have studied the coalescence, or knitting together, of clusters formed in the initial nucleation process as a function of rf plasma power and substrate temperature. Our unique probe provides submonolayer sensitivity to surface relaxation processes on the time scale of ~50 ms. This allows us to study monolayer-by-monolayer growth at rates of 50 Å/s. We identify here the key role that precursor surface diffusion plays in ensuring optimum photoelectronic properties. Equilibrium concepts have suggested that the Si network and the incorporated H behave independently as separate "sub-networks." The surface processes revealed here appear to be necessary in order to establish a well-ordered Si network occupying a deep minimum in configurational coordinate space.

2. Experimental Methods

2.1 Ellipsometric Instrumentation

A description of the unique capabilities of the real time SE system is in order. This system (see Fig. 1) consists of a collimated Xe source, a rotating polarizer, the a-Si:H growth and H

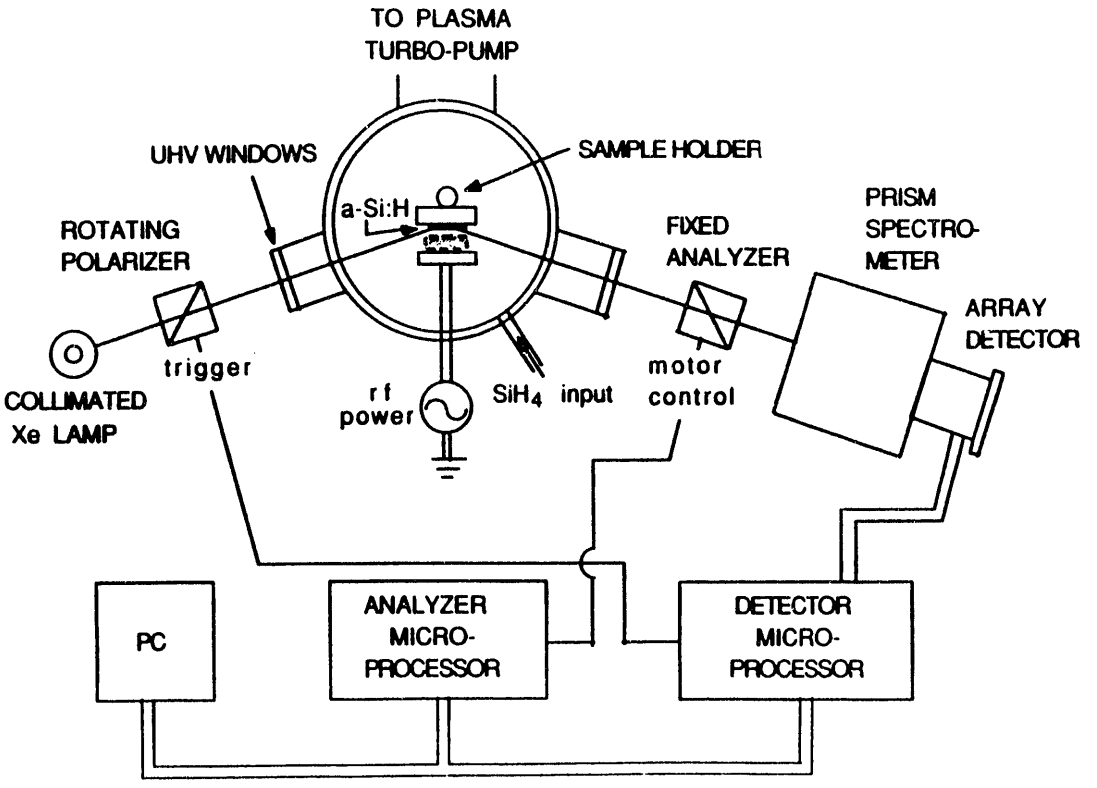

Fig. 1 Experimental apparatus for real time spectroscopic ellipsometry. In this schematic the deposition system is configured for rf plasma-enhanced CVD of a-Si:H.

modification system, a fixed polarizer, and a multichannel detection system [11,12]. The latter consists of a spectrograph, a 1024-pixel Si photodiode array, and its controller. The photodiode pixels are usually grouped by 8 to generate 128 spectral positions from the near-infrared to the near-ultraviolet. Of these, about 100 points span the useful spectral range from 1.5 to 4.5 eV.

To operate the multichannel ellipsometer, the array is read out 4 times per half-mechanical rotation of the polarizer (i.e. one optical cycle) synchronized with an optical encoder mounted on the polarizer motor shaft. From these 4 read outs, full spectra in the ellipsometry angles (ψ,Δ) can be determined. As usual (ψ,Δ) are defined by $\tan\psi=|r_p/r_s|$ and $\Delta=\delta_p-\delta_s$, where $r_p=|r_p|\exp(i\delta_p)$ and $r_s=|r_s|\exp(i\delta_s)$. r_p and r_s are the complex amplitude reflection coefficients of the surface for p- and s-polarized waves. We will not dwell on the determination of physical parameters from (ψ,Δ), but briefly point out the analysis method at different stages in the development below.

At the typical polarizer speed we employ here, 12.5 Hz, a single (ψ,Δ) spectrum can be obtained in a 40 ms acquisition time. In general, we need to average over two consecutive optical cycles to improve accuracy, and over a larger number of cycles to improve precision to achieve a sensitivity of about a tenth of a monolayer. Here acquisition/repetition times for complete pairs of (ψ,Δ) spectra were usually either set at (160 ms)/(1 s) for 4 optical cycle averaging, or (3.2 s)/(15 s) for 80 optical cycle averaging, depending on the desired speed. Acquisition times for selected data will be noted below where pertinent.

2.2 Materials Preparation and Processing

A-Si:H depositions for the study of hydrogen equilibration processes were performed by conventional parallel-plate PECVD. The chamber is uhv compatible, turbopumped to a base pressure of 10^{-8} Torr. Strain-free windows were mounted on uhv flanges for optical access at an angle of incidence of 70°. Pure SiH_4 was used with a flow rate of 20 standard cm^3/min and a gas pressure of 0.2 Torr. The rf plasma power was 2 W, leading to a power flux at the sample surface of 52 mW/cm^2. The sample was mounted at the grounded anode. The substrate temperature was held in the range of 220-250°C. Under these "optimum" conditions, the growth rate was 1.4 Å/s.

Single-side polished silicon wafer substrates were used for the real time SE studies of hydrogen equilibration; double-sided ones were used when infrared transmission measurements of the final films were also desired. For films deposited by alternating growth/equilibration, Corning 7059 glass substrates with predeposited Cr coplanar electrodes were used for electrical measurements; glass substrates without contacts were used for optical transmission and reflection measurements. The results of the latter allowed us to calibrate dual beam photoconductivity measurements to obtain the sub-gap absorption coefficient in the near infrared.

Atomic H treatments were performed in the same chamber, using a tungsten filament 5 cm long and 0.25 mm in diameter. Treatments designed to avoid etching were performed with the filament mounted so as to block a direct line of sight to the sample. Etching was most effective, on the other hand, in a line of sight configuration, presumably owing to a higher flux of atomic H reaching the surface, a higher thermal energy for the H, and/or direct electron impact. The pressure was set from 4 to 8 mTorr for most studies. This comparatively low value avoids thermalization/recombination of the atomic H through collisions. The filament power was used to control the H concentration, and in these studies power levels from 5-40 W were employed. For the thicker a-Si:H films (~2500 Å) studied by real time SE, this power range establishes an equilibrium chemical potential in the near-surface below that at which loss of Si atoms from the surface (i.e. etching) occurs. Further details of the phenomena will be relevant when the results are presented. Finally, the duty cycle for alternating growth and H exposure for the studies of the optoelectronic properties of uniformly equilibrated thick films was established in view of the conclusions of the ellipsometric studies which are sensitive to the near-surface region (top 500 Å) of a-Si:H.

For real time SE studies of thin film coalescence, a wider range of depositions was undertaken. In the conventional parallel plate configuration, the substrate temperature was varied over the range from 120°C to 300°C, and the rf power flux from 52 mW/cm^2 to 780 mW/cm^2. The latter led to an increase in deposition rate from 1.4 Å/s to 11 Å/s. We also studied selected depositions by remote He PECVD at substrate temperatures of 120°C and 250°C. Other conditions for the remote process were: 5/50 stand. cm^3/min flows of SiH_4/He (with the SiH_4 injected downstream), 0.4 Torr total pressure, and 300 mW/cm^3 rf power density for the He plasma. Under these conditions, the deposition rate was 0.08 Å/s Although the majority of these depositions was performed using c-Si wafer substrates, selected parallel-plate and remote He depositions were performed on ultra-smooth sputtered Cr substrates held at 250°C.

3. Post-Hydrogenation Studies of a-Si:H

3.1 An Overview of the Effects of H-Exposure

We need to provide an overview of the phenomena involved in H equilibration first, so that we can justify the use of a specific optical model for interpretation of the real time SE data. Figure 2 shows fits to the infrared absorption spectra collected in both the Si-H bond wagging and bond stretching mode regions for an 0.85 μm thick film prepared by cycling growth with H-exposure as described below. Also shown are the results for a continuously-grown sample. This comparison suggests that the total H content deduced from the wagging mode increases from ~9 at.% to ~13 at.% as a result of the H-treatments. As shown in Fig. 2 at least 80% of

this 4 at.% increase is associated with the bonding configurations that give rise to the 2000 cm^{-1} mode, presumed to be monohydride. The remainder is associated with the 2100 cm^{-1} mode that appears to arise from monohydride configurations associated with surfaces and voids.

Figure 3 shows the absorption spectra of two samples codeposited with those of Fig. 2 plotted from 0.8 to 1.8 eV. These spectra were deduced from a combination of dual beam photoconductivity and optical transmission-reflection measurements when both samples were in the annealed state. Although results such as these will be discussed in greater detail in Sect. 3.11, the main observation to be noted here is that the H-treatments do not lead to an increase in the density of dangling bond defects which give rise to the absorption shoulder at low energies. In fact, if we were to integrate the absorption in excess of the Urbach tail, and apply the correlation between excess absorption and spin density provided by Amer and Jackson [13], then dangling bond defect densities of $5x10^{15}$ cm^{-3} and $7x10^{15}$ cm^{-3} are estimated for the treated and untreated samples of Fig. 3, respectively. Thus, as a model for interpreting the optical-near-ultraviolet dielectric properties we can view the H-treatment process as converting some atomic fraction of the Si-Si bonds to Si-H bonds. It is not clear at this point whether the Si-H configurations are isolated or in complexes [6]. Although the best fits to the Urbach tails provide exponential slopes that reveal a slight decrease (from 49 to 47 meV) upon H-treatment, the effect is not significant. Using the conventional interpretation of the the band tail states as originating from weak Si-Si bonds, we conclude that a measurement uncertainty of ±1 meV in the band tail slope implies an inability to discern a preference factor of < 2 for weak Si-Si bond breaking by H.

3.2 Optical Detection of Bonding Configurations in a-Si:H

In view of the basic ideas presented above in Section 3.1, we can proceed to interpret the ellipsometric spectra. Figure 4 shows a 3-dimensional plot of the change in the imaginary part of the pseudodielectric function as a function of time in the interband region from 2.5 eV to 4.0 eV obtained during a 1 hour H-exposure of previously-untreated a-Si:H. The a-Si:H was prepared under optimum conditions to a thickness of 2500 Å, which ensures opacity over the 2.5 to 4.5 eV photon energy range. During treatment, the a-Si:H was held at its deposition temperature of 240°C, and the H_2 pressure and filament power were 8 mTorr and 28 W, respectively.

The imaginary part of the pseudodielectric function plotted in Fig. 4 is calculated directly from (ψ,Δ) using the following equation:

$$\langle\varepsilon\rangle = \langle\varepsilon_1\rangle + i\langle\varepsilon_2\rangle = \sin^2\theta + \sin^2\theta \tan^2\theta \{[1-\tan\psi\exp(i\Delta)]/[1+\tan\psi\exp(i\Delta)]\}^2, \qquad (5)$$

where θ is the angle of incidence. The pseudodielectric function $\langle\varepsilon\rangle$ reduces to the true

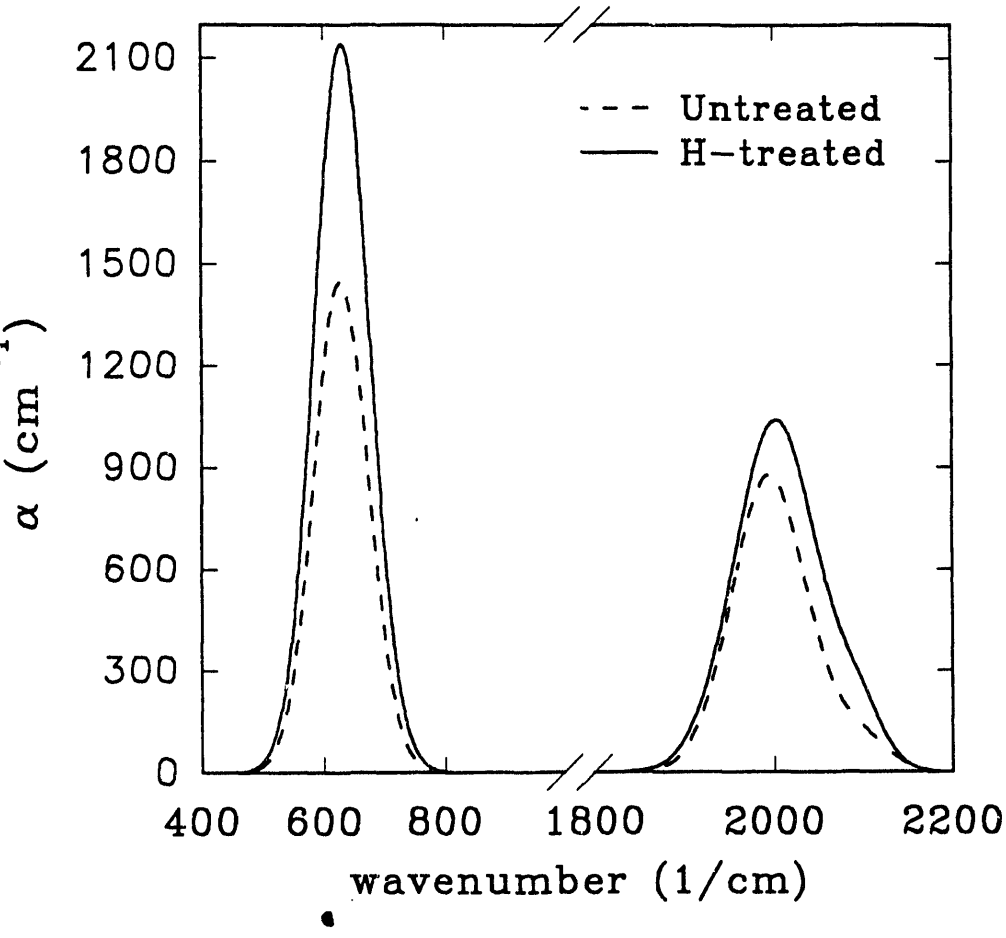

Fig. 2 Fits to infrared absorption spectra in the Si-H bond wagging and bond stretching regions for PECVD a-Si:H deposited on c-Si at 220°C. The solid line was obtained from a sample prepared by alternating a-Si:H growth with exposure to a H_2 atmosphere enriched with hot filament-generated atomic H to obtain an a-Si:H film 0.85 μm thick. The broken line was obtained from a control sample, prepared under identical conditions to the same thickness, but in the absence of the H-treatment. See Sect. 3.11 for details.

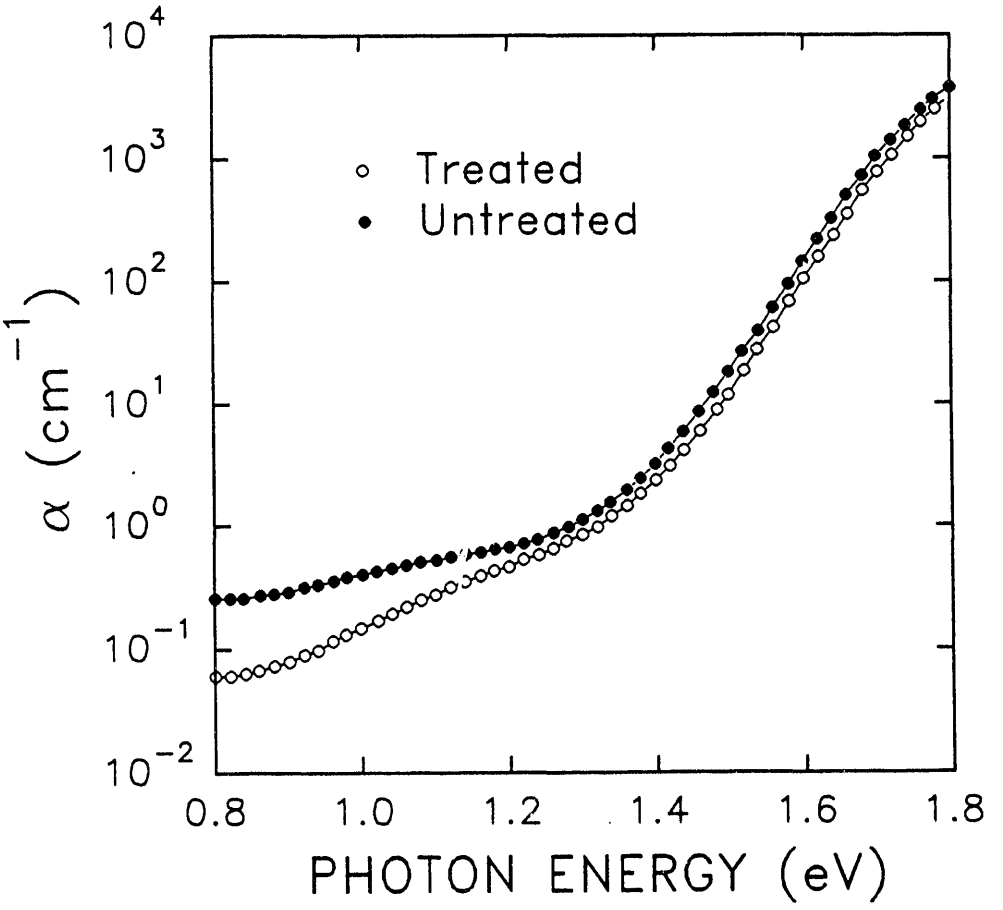

Fig. 3 Absorption spectra obtained from 0.8 to 1.8 eV using a combination of dual beam photoconductivity, transmittance, and reflectance measurements for PECVD a-Si:H films codeposited with those of Fig. 2. See Sect. 3.11 for details.

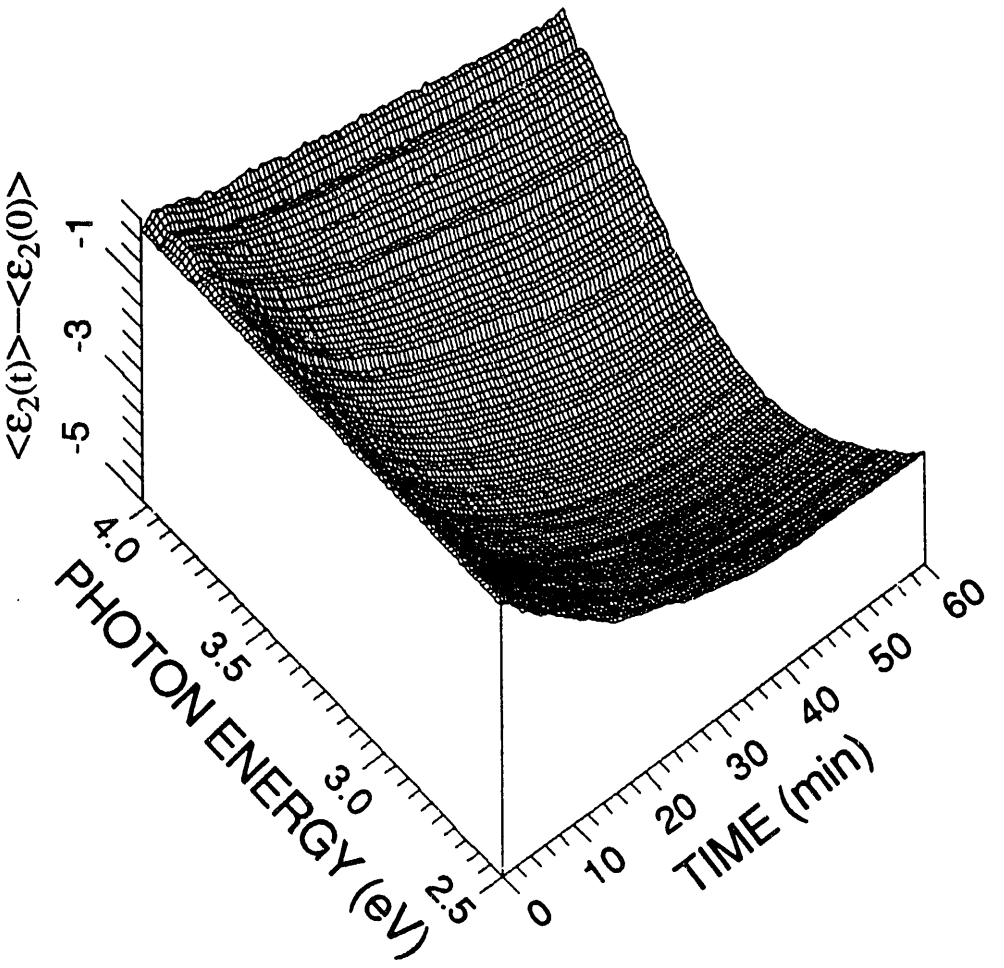

Fig. 4 Three dimensional plot of the change in the imaginary part of the pseudo-dielectric function collected in real time during exposure of a 2500 Å thick film of optimum PECVD a-Si:H to atomic H generated by a heated filament. Full spectra were collected every ~15 s over the one hour exposure time. The H-treatment was performed immediately after film growth on c-Si at 240°C, and during the treatment the a-Si:H was held at the deposition temperature.

dielectric function ε when the material under study is opaque and its surface is atomically smooth and clean.

Figure 5 (solid line) shows the dielectric function $\varepsilon=\varepsilon_1+i\varepsilon_2$ of the film obtained at the temperature of deposition, 240°C, prior to the H-treatment. The imaginary part of the dielectric function exhibits the strong, broad peak centered at 3.75 eV, corresponding to the polarizability of Si-Si bonds. This was extracted from pseudo-dielectric function data, after correcting for a roughness layer of thickness 10 Å. The roughness thickness was determined from real time SE data collected during bulk film growth in the regime of semitransparency. Such data were interpreted by an extension of linear regression analysis, that provides the surface roughness and bulk layer thicknesses and the assumed thickness-independent bulk film dielectric function [14]. (For an example of the outcome of such an analysis, see Fig. 23.)

Similarly, we can extract the dielectric function of the film at the end of the H-treatment, but only if the following two assumptions hold. (1) The surface roughness thickness or the roughness microstructure must not change, and (2) the modification of the optical properties that results from Si-Si bond conversion to Si-H (see Fig. 4) must occur uniformly throughout the penetration depth of the light. To provide some sense of assumption (2), Figure 6 shows the optical penetration depth; i.e. the depth at which the irradiance drops by a factor of $e^{-1}=0.36$ within the material. (Here we use normal incidence since the multiplicative factor, $\cos\theta_t$, which accounts for the non-normal angle of transmission, θ_t, is near unity owing to the high index of refraction of a-Si:H.) Thus, Si-Si bond conversion must occur uniformly at least to a depth of ~500 Å in order to extract the true dielectric function over the 2.5 to 4.5 eV range. If uniformity is achieved to a depth of 200 Å, on the other hand, then the true dielectric function can be extracted only over the 2.9-4.5 eV range.

Below, we will demonstrate that assumption (1) is valid; however, assumption (2) may introduce some errors in the analysis of data collected during hydrogenation at 240°C. These errors will be assessed in greater detail below. Because assumption (2) does break down more severely as the hydrogenation temperature is reduced, only the data collected at 240°C are utilized to extract the dielectric function of the film at the end of H-treatment.

Figure 5 (broken line) includes the dielectric function of the material modified by 1 hour of H-treatment, deduced on the basis of the above assumptions. It should be recalled that after 1 hour treatment, the pseudo-dielectric function has saturated over the full 2.5 to 4.5 eV spectral range. The overall effect of the H-treatment on the dielectric function is roughly similar to that expected if some volume occupied by Si-Si bonds is removed and replaced by void volume. This in turn would remove oscillator strength uniformly from the broad peak centered at 3.75 eV as shown from the theoretical spectra of Figure 7, which were calculated from the Bruggeman effective medium theory [10]. Clearly, the void model works well if the Si-Si bonds are broken and passivated in such a way that the associated electronic transitions are shifted beyond the high

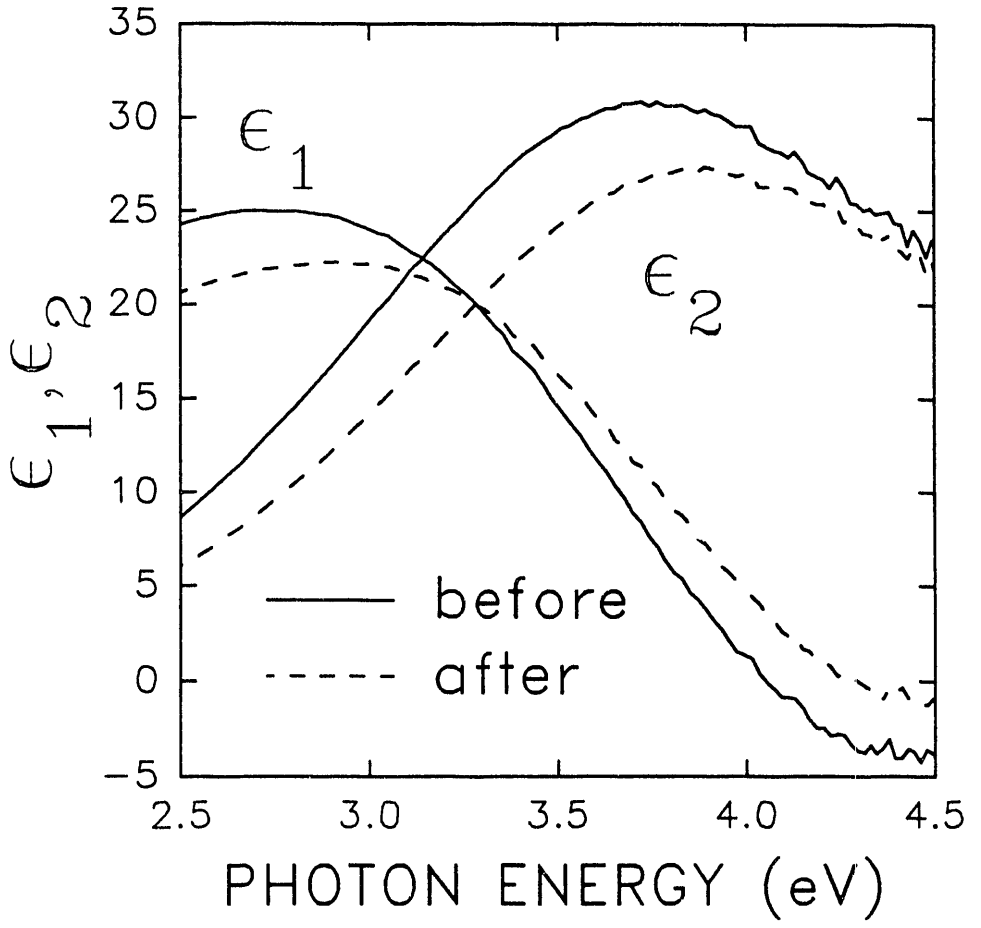

Fig. 5 Dielectric function from 2.5 to 4.5 eV for a 2500 Å thick a-Si:H film deduced from an analysis of the real time SE data of Fig. 4, collected at the end of the deposition (solid lines). Corresponding results (broken lines) were obtained after a one hour exposure of the same sample to filament-generated atomic H. The processing and measurement temperatures were 240°C. In order to obtain true bulk dielectric functions, a 10 Å surface roughness layer was extracted in both cases.

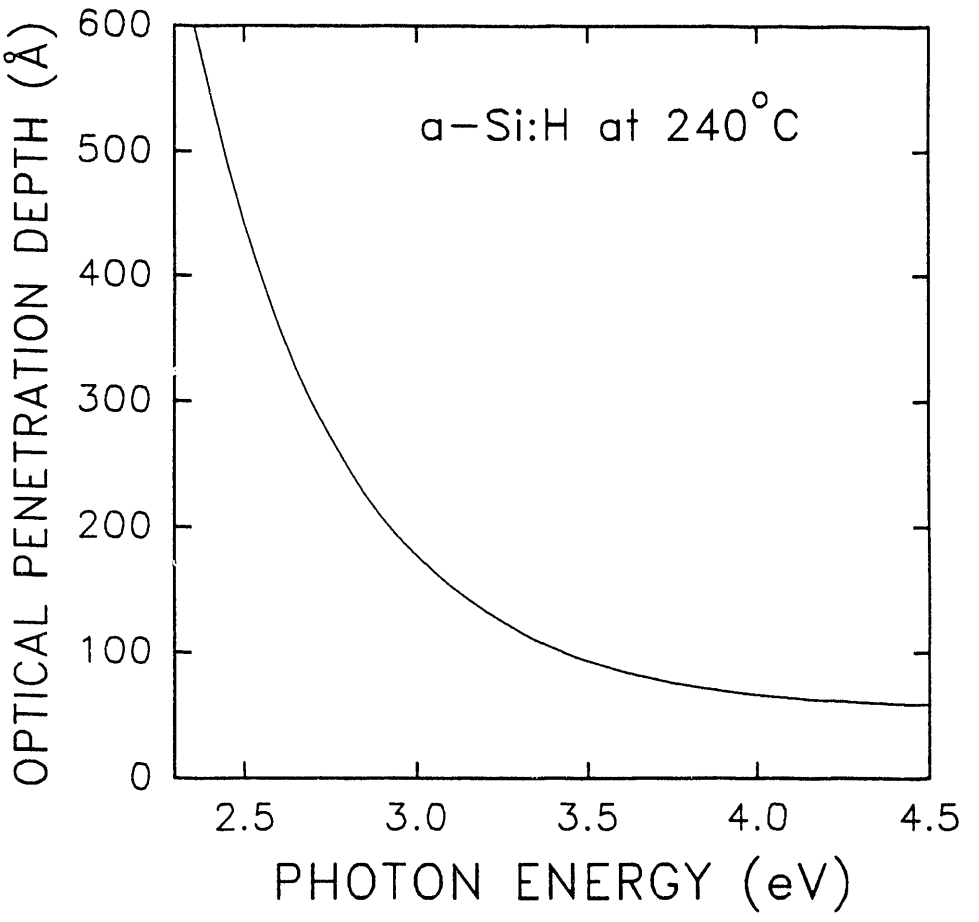

Fig. 6 The optical penetration depth, or the reciprocal of the absorption coefficient, for optimally-prepared a-Si:H (with 8-9 at.% H) at a measurement temperature of 240°C, plotted as a function of photon energy from 2.5 to 4.5 eV.

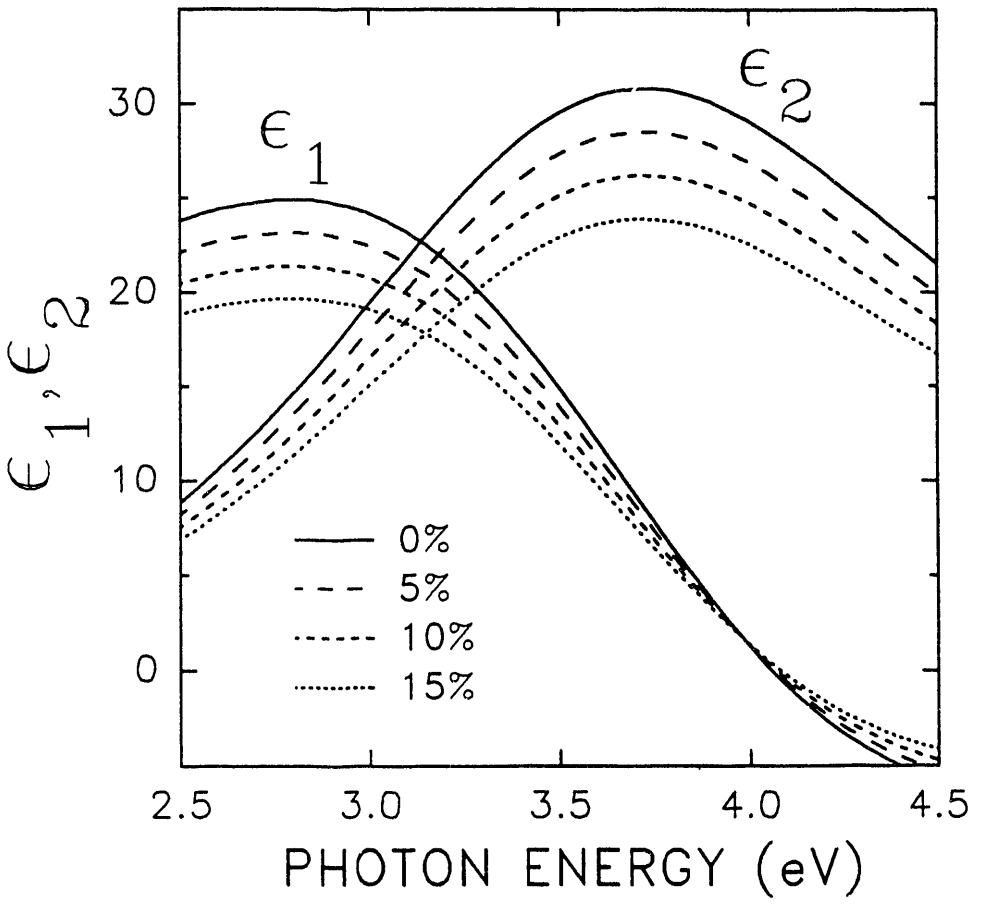

Fig. 7 The dielectric function of amorphous silicon having different percentages of voids by volume. These results were calculated from the two-component Bruggeman effective medium approximation, where one component was the material labelled 0 vol.% and the second component was free space [$(\varepsilon_1,\varepsilon_2)=(1,0)$].

energy limit of our system. However, in the case of Fig. 5, the ε_2 maximum does not remain fixed as in the void model calculation of Fig. 7, but rather increases to higher energy. This is consistent with the conversion of Si-Si bonds to Si-H bonds whose associated electronic transitions are higher in energy, but not outside our experimental energy window.

In an attempt to better quantify this behavior, we assume that the final material after H-treatment is a microscopic composite consisting of two components (measured in terms of their volume fractions). Component A has optical properties identical to the original sample, and component B represents the material converted by the H-treatment. Within this model, the dielectric function of component B is uniquely defined by the two dielectric functions in Fig. 5, as long as we add one reasonable constraint: ε_2 for this component must gradually approach zero at the lower photon energies. Figure 8 shows the final result (points) along with a fit to the Forouhi-Bloomer model [15] for the dielectric function of an amorphous semiconductor (solid line). The close fit achievable shows that dielectric function passes an important test required of true optical functions: it satisfies the Kramers-Kronig relationship. Thus, as an outcome of our work, we believe we have identified the optical properties characteristic of monohydride bonding groups, although we expect some minor contribution to the results due to other bonding configurations.

Such a decomposition of the dielectric function of the H-treated a-Si:H, is based on the assumption that oscillator strength is removed homogeneously from the Si-Si bond transitions. However, we expect that the spread in the energies of the broken Si-Si bonds (<0.2 eV) is small compared to the overall width of the peak in ε_2 (~2 eV), the latter being controlled by other factors, namely the bandwidth in the joint density of states and the relaxation times for the transitions. Thus, if weaker Si-Si bonds are preferentially attacked by H, our analysis is not invalidated. Conversely, the optical probe can detect Si-Si bond breaking irrespective of the strength of the bond.

To understand better the results of Figure 8, we next consider the fact that, for the H-modified material, obtained after saturation of the pseudodielectric function and equilibration of the near surface region, 24 vol.% of the original material has been converted to the Si-H component. As described in Section 3.8, a few vol.% of the Si-H component is unstable, however, and reverts back to the original structure when the atomic H source is removed and the sample is annealed at the treatment temperature for a number of hours (see Fig. 19 below). As described in Sect. 3.1 (see Fig. 2), infrared absorption studies of thick a-Si:H prepared by alternating optimum growth with H-treatment (and subjecting the film to a final anneal at the treatment temperature) suggest that an additional 4 at.% H is incorporated into the a-Si:H through the equilibration process. The fact that 4 at.% H influences ~20% of the volume shows that the fundamental unit of polarizability (of which the dielectric function in Fig. 8 is a characteristic) is not the Si-H bond itself but rather a larger unit such as the Si-Si_3H (Si-centered)

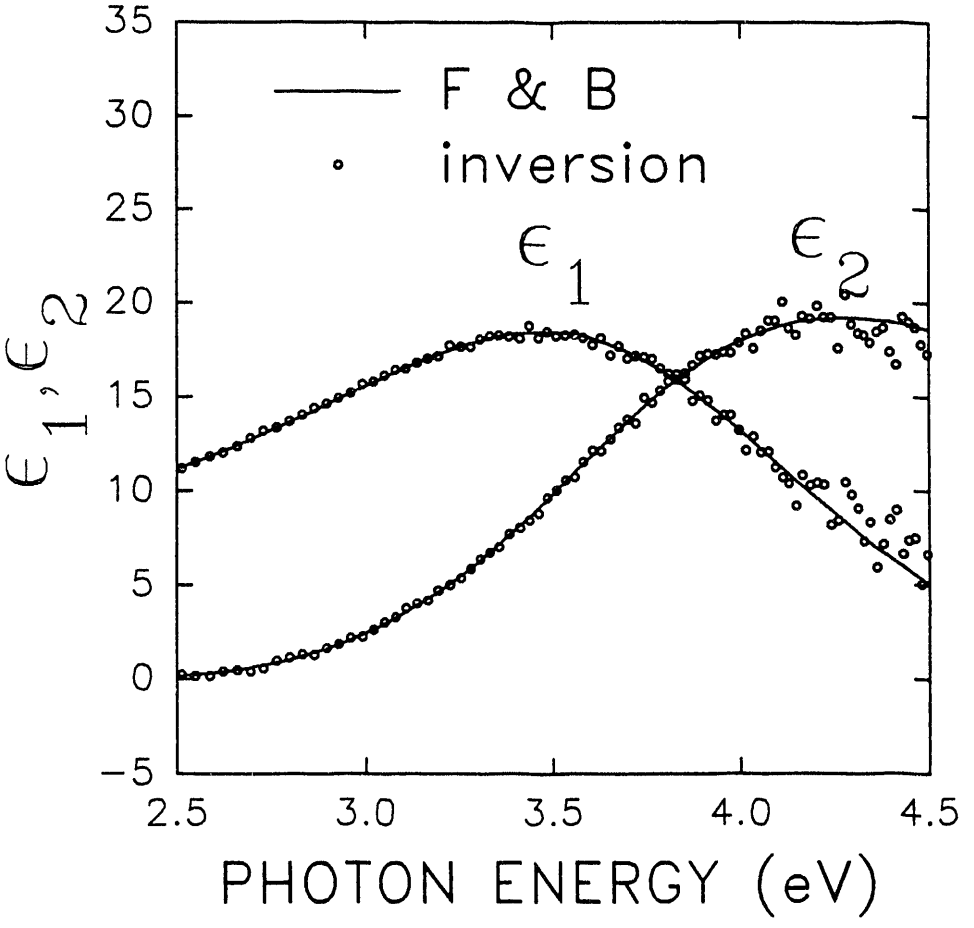

Fig. 8 Dielectric function for the Si-H bonding component introduced into a-Si:H upon atomic H exposure of optimum PECVD a-Si:H (points). These results were obtained from the spectra in Fig. 5, applying the Bruggeman effective medium approximation, and are appropriate for the measurement temperature of 240°C. The solid line is a fit to the analytical formulae of Forouhi and Bloomer, which satisfy the Kramers-Kronig relationship.

tetrahedron [16]. Any underestimate in the bonded H-content (e.g., due to non-uniformity in the alternating growth/treatment materials) scales down our size estimate of the fundamental unit, but the general conclusion reached here is well outside possible errors.

In addition to their fundamental impact, the results obtained here will be applied in the next part to develop a better understanding of the diffusion and reaction processes through an analysis of SE data collected in real time. With the optical signature of the excess Si-Si_3H bonding configurations (henceforward called the "Si-H component"), we can interpret real time SE data using multilayer optical models, in some cases simulating the SE data expected for H-diffusion, and in other cases fitting the observed data to Si-H component profiles. In effect, this allows us to perform the first real time studies of H-diffusion in the atomic H environment. However, we must interpret our SE observations with care. First, unlike SIMS, our optical measurements are not expected to be sensitive to any unbonded H or H_2. In addition, as just noted, our optical approach lacks the specificity to sense directly the conversion of Si-Si bonds of different strengths, or the formation of Si-H bonds in complexes. Any inferences that we make are based on different kinetic behavior of the trapping and emission of free H. Because of the limitations of SE, it is important to perform ex situ measurements of the H-modified materials as well.

3.3 Equilibration of the Chemical Potential in a-Si:H: Simulations of Expected Behavior for a Diffusion-Limited Process

In Figure 4 we showed the decay of the imaginary part of the pseudo-dielectric function during a heated filament H-exposure of one hour's duration. Selected spectra from 2.5 to 4.0 eV for both optical parameters, obtained during the same process are shown in Fig. 9. In this case, the parameters (ψ,Δ) are plotted because an inspection of the change in Δ provides information on changes in surface morphology. Figure 10 shows the effect of surface roughness layers (each modeled as a 0.5/0.5 volume fraction mixture of bulk a-Si:H and void) on the Δ spectrum over the same photon energy range. By inspection of the data in Fig. 9 in comparison with Fig. 10, it is clear that under our H-treatment conditions, the surface roughness thickness change is restricted to less than a single monolayer (~2 Å) over the full hour exposure. Thus, the first of the two assumptions made to deduce the dielectric function of Fig. 8 is correct. With this result, we emphasize an important capability: hydrogenation with negligible surface reordering due to etching.

Next, in order to understand the process by which Si-H bonds are formed in the a-Si:H during H-treatment, we calculate the expected real time SE spectra for a situation in which the additional H is incorporated in a diffusion-limited process. As one specific mechanistic model, H from a surface Si-H bond may be released and diffuse below the surface as an interstitial until it is trapped at a weak Si-Si bond site and is immobilized for the remainder of the

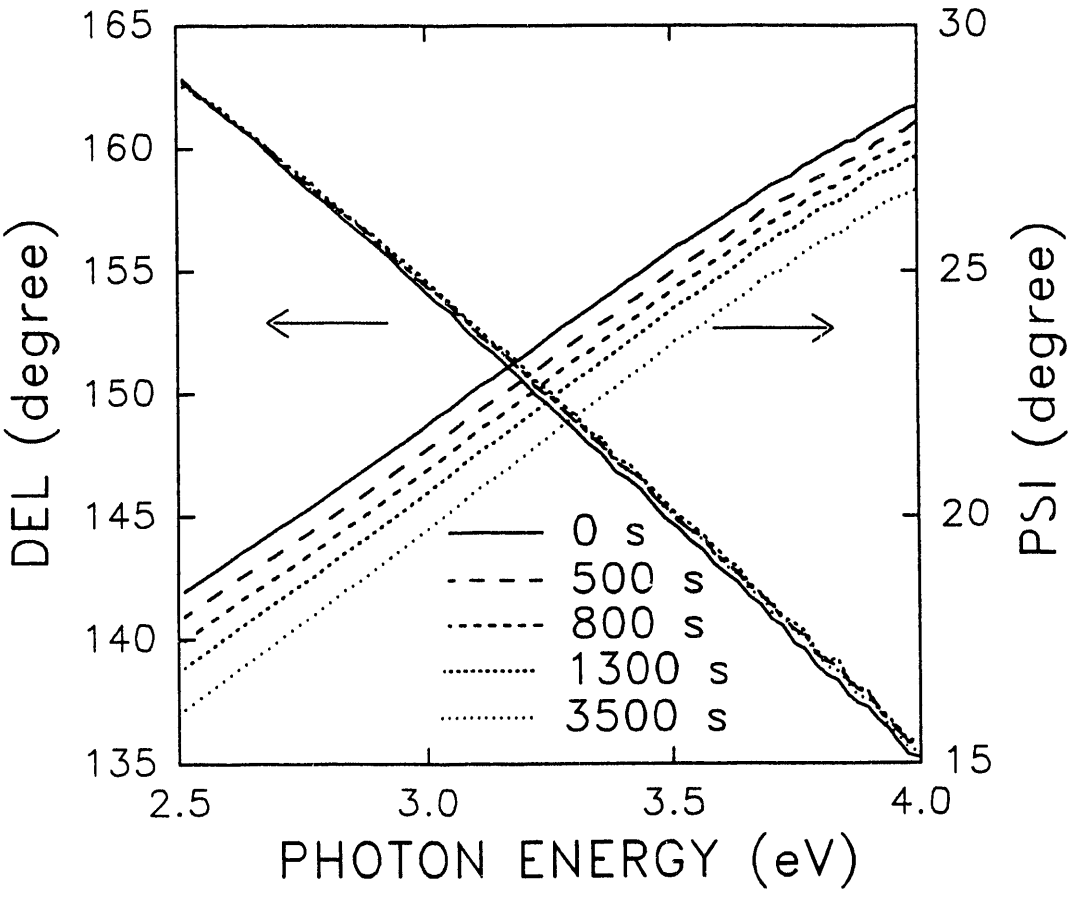

Fig. 9 Experimental spectra in the ellipsometry angles (ψ,Δ) at selected times during a one-hour exposure of optimum a-Si:H to filament-generated atomic H. The a-Si:H was maintained at a temperature of 240°C during treatment. This sample is that same as that depicted Figures 4 and 5.

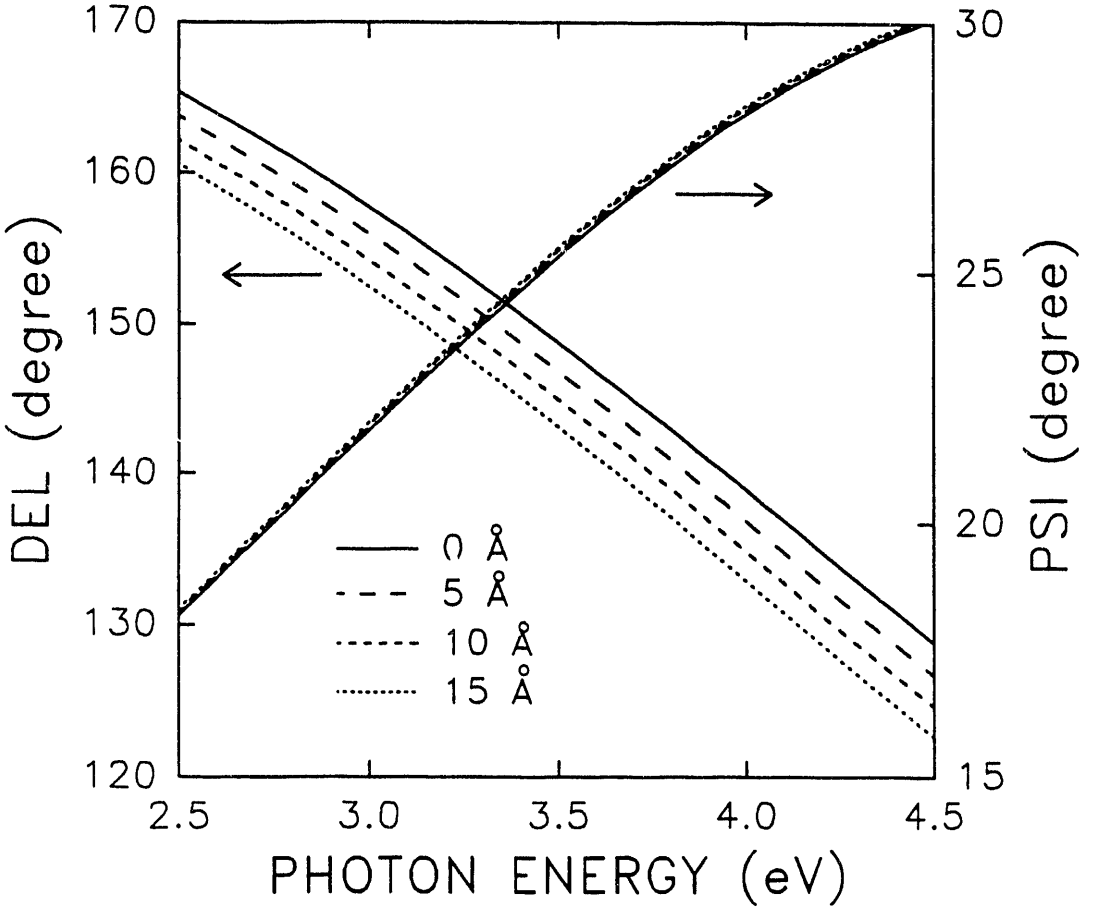

Fig. 10 Simulated (ψ,Δ) spectra for opaque a-Si:H at 240°C, showing the effect of surface roughness layers of different thicknesses. The roughness layer in each case was modeled using the Bruggeman effective medium approximation as a 50/50 vol.% mixture of bulk a-Si:H and void.

experiment [17]. This leads to a Si dangling bond and an Si-H bond, reaction products that would be detectable by SE through the change in optical reponse. The second dangling bond would eventually be terminated by a second diffusing H. In this process, one might expect the local volume fraction, f, of the Si-H component to reflect the diffusion profile:

$$f(x,t) = f_0 \, \mathrm{erfc}\{x/[2(D_H t)^{1/2}]\} \qquad (6)$$

where "erfc" is the complementary error function, D_H is the diffusion coefficient, and f_0 is the long time equilibrium Si-H component volume fraction. The latter value is 0.24 in the experiment of Fig. 9, as discussed above in connection with the optical model of Fig. 8. Although H diffusion in a-Si:H is found to be dispersive [9], through secondary ion mass spectrometry (SIMS) measurements of hydrogenated/deuterated a-Si multilayers, it is not necessary to include this feature in our development at this time.

Figure 11 shows a snapshot of typical Si-H volume fraction vs. depth into the sample at different times for a diffusion coefficient of 1×10^{-16} cm^2/s. The vertical (dot-dash) lines show how this Si-H profile was sliced into a multilayer structure for the purposes of simulating the ellipsometric spectra for comparison with Fig. 9. Within each slice the Si-H component was fixed as the average of the two values at the boundaries of the slice. Figure 12 shows the final result of this calculation at the four different times coinciding with those plotted in Fig. 9. It is clear that a significant change in Δ occurs in the simulation that is absent in the data. This change in Δ is attributed to the movement of the diffusion front [e.g. defined by $x=(D_H t)^{1/2}$] passing through our window of observation which in this case is the penetration depth of the light.

The question then arises as to whether our data are characteristic of a much higher diffusion coefficient than that from the SIMS studies of hydrogenated/deuterated multilayers. If so, then the diffusion front might pass through our window of observation faster than we could detect it. Figure 13 addresses this point; it shows (ψ,Δ) data versus time at a fixed photon energy of 3.0 eV, collected in a separate experiment with a faster data acquisition rate, but under identical H-treatment conditions as in Fig. 9. In Fig. 13 the data are compared with simulated results for diffusion coefficients of 10^{-16} and 10^{-14} cm^2/s. It is clear that the observed constant value of Δ and the slowly decreasing ψ are incompatible with any model which involves Si-Si bond breaking limited by diffusion of H to the site. Thus, we note that our data are inconsistent with the conventional view of H motion.

3.4 Reaction-Limited Equilibration of the Chemical Potential in a-Si:H

An approach that can fit the nearly time-independent Δ value is to assume that Si-Si bond breaking by H insertion occurs with a time-independent profile shape, i.e. $f(x,t)=g(x)h(t)$,

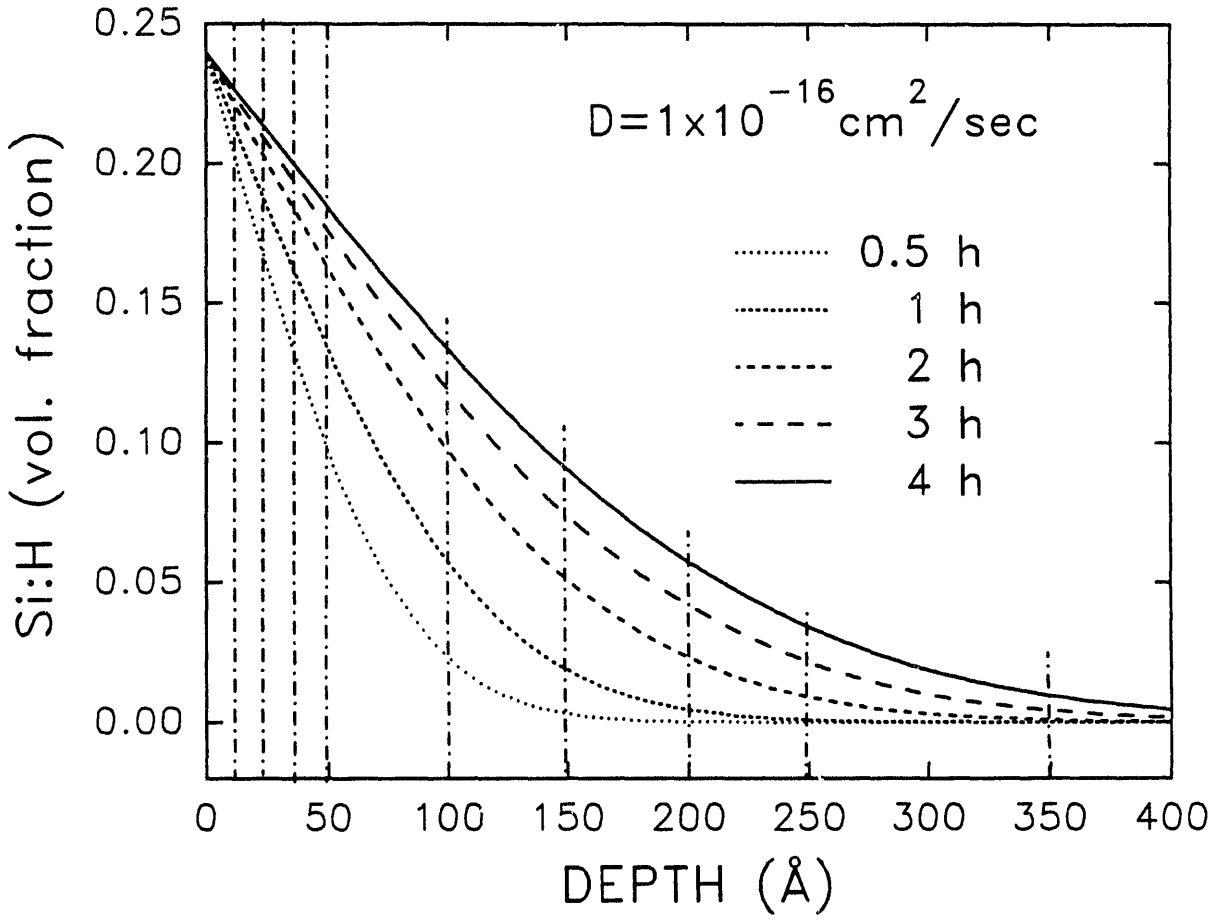

Fig. 11 Snapshots of the error-function profile for the Si-H component volume fraction calculated assuming diffusion-limited behavior with a diffusion coefficient of $1x10^{-16}$ cm^2/s and a volume fraction of 0.24 at equilibrium. This choice for the diffusion coefficient is based on literature measurements of H diffusion by SIMS in hydrogenated/deuterated multilayer structures. The vertical lines denote slices used in an optical simulation of the profiles that permit multilayer optical calculation of the ellipsometric spectra for a sample having this Si-H component profile. The Si-H component fraction in each slice is the average between the values at the boundaries of the slice.

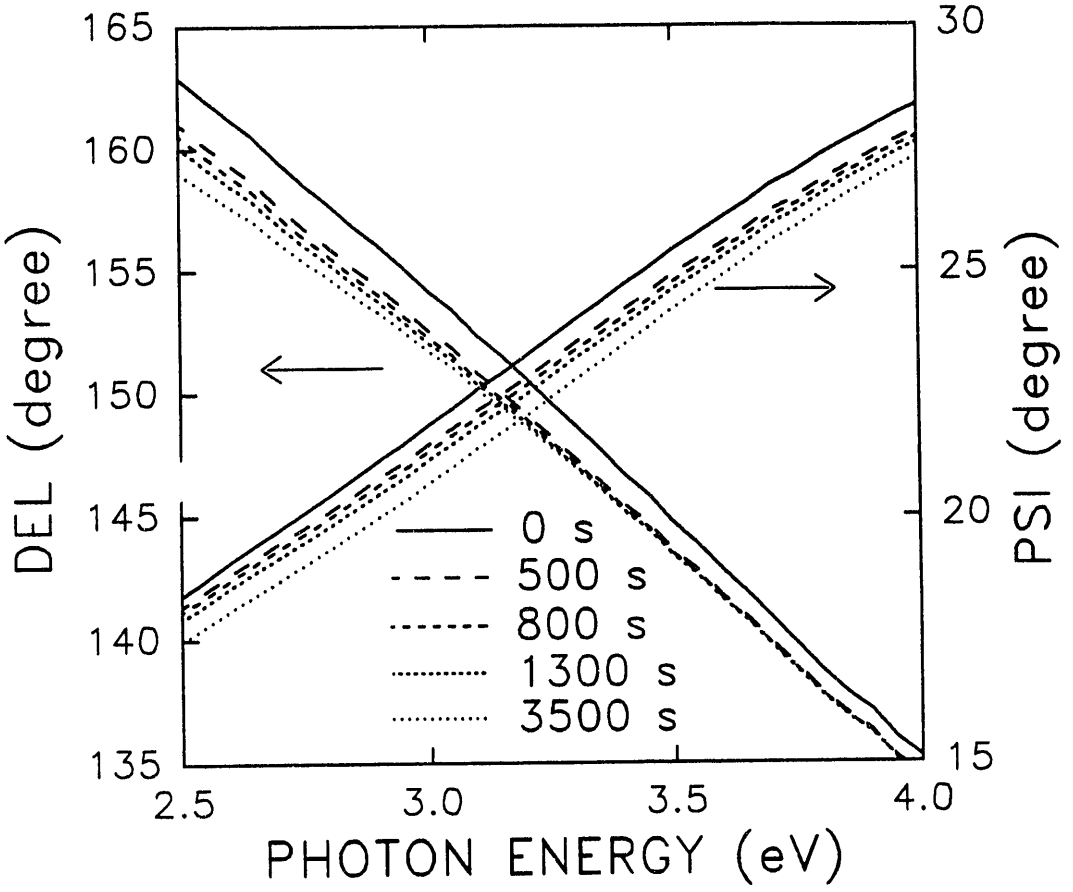

Fig. 12. Simulated (ψ,Δ) spectra at different times for a-Si:H calculated from diffusion profiles such as those in Fig. 11, assuming a diffusion coefficient of 1×10^{-16} cm^2/s and an equilibrium Si-H component volume fraction of 0.24. These spectra are to be compared with the experimental results in Fig. 9 to assess diffusion-limited behavior.

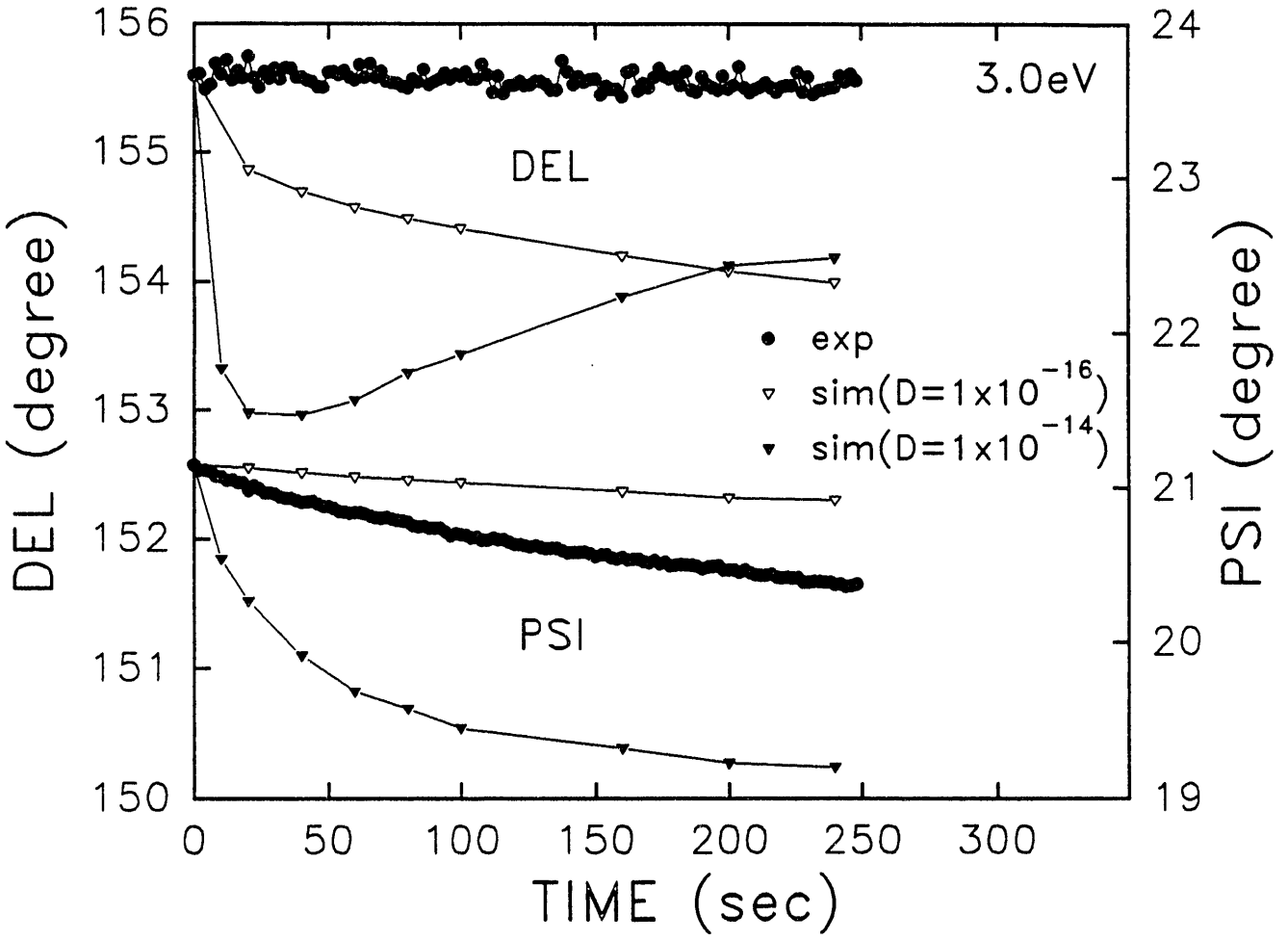

Fig. 13 Experimental ellipsometric angles (ψ,Δ) at a photon energy of 3.0 eV collected versus time at 1 s intervals during the exposure of optimum PECVD a-Si:H to atomic hydrogen at a temperature of 250°C (solid circles). The open and solid triangles show the results of simulations calculated from diffusion profiles such as those in Fig. 11 assuming diffusion coefficients of 10^{-16} and 10^{-14} cm^2/s, respectively.

throughout the penetration depth of the light for all photon energies. Figure 14 shows the ellipsometric simulation of such a situation for comparison with the data of Fig. 9 when a constant profile is assumed, i.e. g(x)=constant. When the uniform volume fractions of the Si-H bonded component are chosen as 5, 10, 15, and 24 vol.%, the simulation matches the data closely for all four times in Fig. 9. From this, we suggest that the process of Si-Si bond breaking by H is "reaction-limited". Within this classification, we include two possibilities: (1) an energy barrier for the formation of the Si-H component determines the reaction rate; or (2) no barrier is present and the H- capture or trapping event determines the rate. Implicit in this result is the fact that the diffusion process whereby H reaches the reaction site is undetectable by the optical probe. This may suggest that the time-averaged concentration of diffusing H (over ~1 s measurement time) is too low and/or the diffusing H configuration has a weak optical response (see Sect. 3.5).

Preliminary high resolution SIMS measurements obtained on a-Si:H deuterated at 240°C for two different times (20 and 60 min) support the conclusions deduced optically from SE. In particular, a nearly constant D-profile is observed to a depth of 200 Å that builds up as a function of time. The profile, however falls more sharply after dropping by a factor of two by 300 Å. This result suggests that our second assumption used to deduce the Si-H component dielectric function of Fig. 8 is valid only over the 2.9-4.5 eV spectral range. Because of the overall close fit of the Si-H dielectric function to the predicted analytical form of Forouhi and Bloomer (see Fig. 8), it appears that any errors from 2.5 to 2.9 eV that arise from the breakdown of the assumption of uniformity for depths greater than 200 Å, are small.

If the reaction that generates the Si-H component were to occur only in the forward direction and with a single rate coefficient, α, the volume fraction of the Si-H component, f, should exhibit the following relationship

$$f(x,t) = f_o(1 - e^{-\alpha t}). \qquad (7)$$

within the top 200 Å. The volume fraction, f, can be deduced from the experimental data of Figure 9 using linear regression analysis fitting. The result is plotted logarithmically as $[1-(f/f_o)]$ in Fig. 15 in order to determine the rate coefficient. Very good linear behavior is obtained with a rate coefficient of 8×10^{-4} s^{-1}, thus supporting the concept of "reaction-limited" Si-Si bond breaking to explain the SE results. Drawing an analogy with electronic processes, we can say that the build-up in the Si-H component reflects deep-trapping of H at centers that (as we shall see) immobilize the H for the *longest* time scale used in our experiments (~10^5 s, see Sect. 3.8). Deviations from linearity in Fig. 15 are typical behavior for more than one rate coefficient, as would be expected for more than one site or pathway for H trapping.

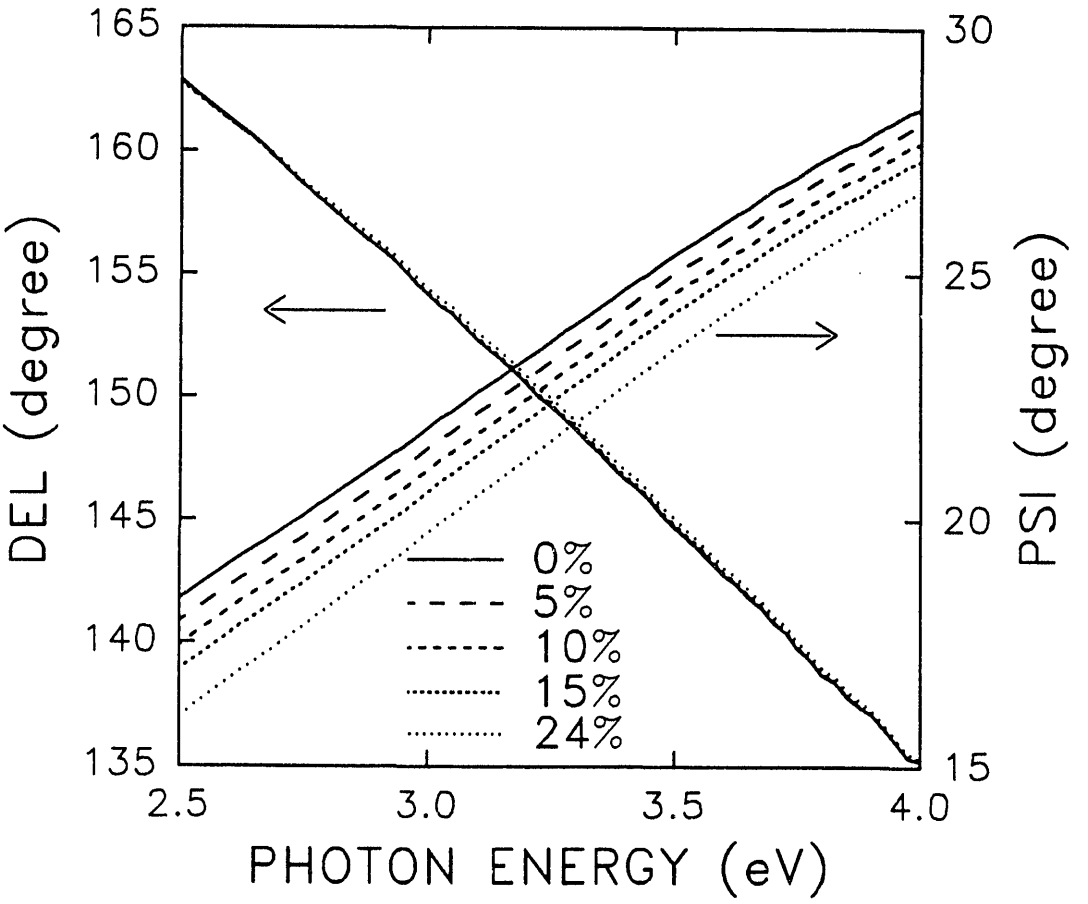

Fig. 14 Simulation of (ψ,Δ) spectra assuming the conversion to Si-H bonding occurs uniformly throughout the sample. The values indicate the volume percent of the original material that is converted to the Si-H component. These calculations are to be compared with the experimental data in Fig. 9.

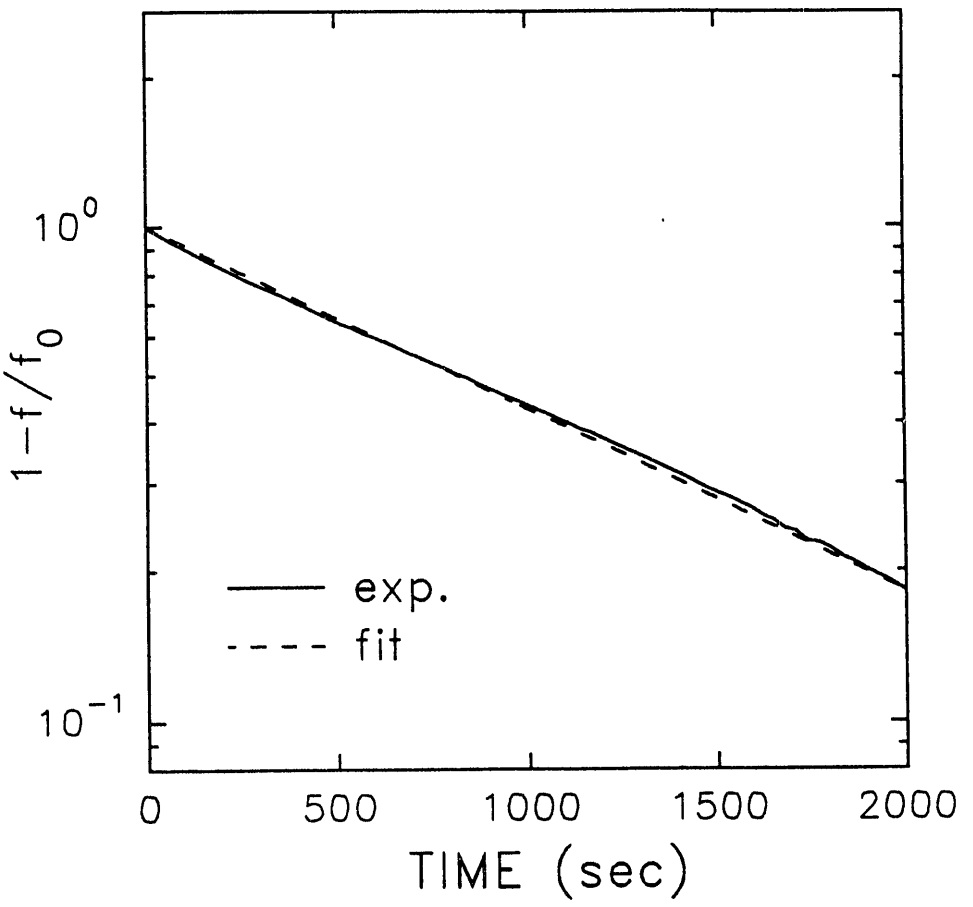

Fig. 15 Volume fraction of the bulk Si-H bonding component, f, expressed as $[1-(f/f_0)]$, deduced versus time from the ellipsometric spectra of Fig. 9 collected during ~1/2 hour exposure of a-Si:H to atomic H (solid line). The sample was maintained at 240°C. The broken line is a fit to a single capture rate, leading to a value of 8×10^{-4} s^{-1}.

3.5 General Model for the Modification of a-Si:H by Atomic H

Two speculative mechanistic models for the overall diffusion-reaction process can be based on the following [17]:

$$H_I + \text{Si-Si} \rightarrow [\text{Si-H} + D^0], \quad (8)$$

$$\text{Si-H-Si(a)} + \text{Si-Si(b)} \rightarrow \text{Si-Si(a)} + [\text{Si-H} + D^0]. \quad (9)$$

In reaction (8), Si-Si bonds react in a diffusive flux of interstitial hydrogen (H_I). In reaction (9), the hydrogen diffuses in a bridge-bonded, bond-centered, or "bond-switching" configuration; there is a finite probability, that the "occupied" bond will remain broken, depending on its local environment, resulting in H immobilization over a measurable time (>1 s). In both reactions the first reactant on the left denotes the diffusing H configuration, and in both cases the product is an [Si-H+D^0] configuration, which is expected to convert to 2[Si-H] with the association of another H. In fact, association with the second H may occur as part of the trapping event or after a certain time interval. It would seem that the difference between the two (8) and (9) would be difficult to detect in any measurement; results presented in Section 3.7 provide further insights into this issue.

Let us call C_d the concentration of the diffusing species occupied by H (i.e. free or shallow-trapped H) and, C_r, the concentration of the product (i.e. deep-trapped H). In fact, there is a demarcation level that separates these two populations, given by $\Delta E=kT\ln(\alpha_{oe}t)$, where t is the time scale over which the Si-H component saturates (~10^4 s), and α_{oe} is an attempt frequency (assume 10^{12}-10^{13} s^{-1}) for emission. In our typical experiments with a time scale of 1 to 10^4 s deep H-traps in fact have depths larger than ~1.8 eV. The spatial and temporal distribution of the these concentrations are controlled by the following coupled equations:

$$\partial C_d/\partial t = -\alpha_r C_d (C_{ro}-C_r) + D_d[\partial^2 C_d/\partial x^2], \quad (10)$$

$$\partial C_r/\partial t = \alpha_r C_d (C_{ro}-C_r), \quad (11)$$

where C_{ro} is the equilibrium concentration of the deep-trapped H at the imposed gas phase chemical potential. D_d is the diffusion coefficient of the diffusing species, and α_r is the rate coefficient for reaction (deep-trapping). We can write $\alpha_r=\alpha_{or}\exp(-\delta E_r/kT)$ where δE_r is the energy barrier in the trapping process. The prefactor α_{or} is an "attempt-to-trap" rate, given by $\alpha_{or}=4\pi r_c D_d$ where r_c is the radius of the trap.

In Eqs. (10-11), we have assumed that the reactions progress only in the forward direction on the time scale of our dynamic measurements, meaning that most of the Si-H component detected optically originates from deep-trapped H that is not reemitted on the longest time scale of

our typical measurements (10^4 s). Quantitatively this means that the emission rate α_e must be much smaller than $\alpha_r C_{do}$, where C_{do} is the surface concentration of free H at the gas phase chemical potential. Studies of H emission from traps in the absence of the diffusing H justifies this assumption, as discussed in detail in Sect. 3.8. Finally, in Eqs. (10-11) we assume that the diffusion coefficient of the reaction product is small in comparison to the diffusing H at the left in reactions (8) and (9). In effect this means that the H cannot tunnel from its original deep trapping site.

It is not necessary to solve Eqs. (10) and (11) in the general situation. It would not be helpful anyway because the depth averaging provided by SE is too large. To make connection with the experimental observations made so far, we consider "reaction-limited" behavior. This occurs at depths into the a-Si:H, x, such that the inequality

$$(\alpha_r C_{do})^{-1} > x^2/D_d \tag{12}$$

holds, When the relationship (12) holds for a given depth x, then the equations become decoupled with diffusion occurring on a faster time scale than reaction. Specifically, the diffusion term in Eq. (10) vanishes, and C_d in Eq. (11) is replaced by the constant C_{do}. Then consistency with our experimental observations is obtained by assigning α in Eq. (7) according to $\alpha=\alpha_r C_{do}=4\pi r_c D_d C_{do}\exp(-\delta E_r/kT)$. Applying Eq. (12) to our experimental situation with $\alpha_r C_{do}=8\times10^{-4}$ s^{-1} and x=500 Å as the depth to which reaction-limited behavior is observed experimentally (as indicated by the time independent value of Δ in Fig. 9), then we find that $D_d>2\times10^{-14}$ cm^2/s. This is a necessary condition for the observed behavior, and does not depend on the specific mechanistic model chosen.

In the most general situation, the detectable optical information may include a contribution not only from the deep-trapped species, but also from the diffusing species which consist of free and/or shallow-trapped H. Thus, the volume fraction representing the optical change, f, can be expressed very crudely as a function of C_d and C_r by $f=\eta_d C_{do}+\eta_r C_r$, where the η_i represent the optical coupling efficiencies of the diffusing and reacted species. It is clear, however, that in order to explain our data in Figs. 9 and 13, the term $\eta_d C_{do}$ must be below our detection limits. If this were not so then a diffusion coefficient $D_d>2\times10^{-14}$ cm^2/s would predict an initial rapid change in ψ as shown in the simulation of Fig. 13. Thus, there are two alternatives, namely the diffusing species are undetectable because of a weak optical response (η_d small) or because of a low time-averaged (~1 s) concentration, i.e. less than 0.5 vol.% (C_{do} small).

The major result of this Section is as follows. The diffusion coefficient of the H species that leads to Si-Si bond breaking in a-Si:H under atomic H exposure is more than two orders of magnitude higher than that obtained in SIMS studies of hydrogenated/deuterated multilayers and the buildup of bonded Si-H is limited by the H trapping event not by H diffusion to the site. We

believe that results of this study and the previous SIMS studies are both correct, and the differences arise from the conditions of measurement. In our case H is injected into the transport level and diffusion is driven by differences in chemical potential. Street et al. [17] have also recognized that the deduced diffusion coefficient may be sensitive function of the measurement approach. We suggest that our approach is more relevant for the growth environment, and because of this our results have important implications for the growth mechanism. We can apply the same argument presented in the introduction concerning the H kinetics during growth, namely that the chemical potential in the sub-surface zone of thickness $L=D_H/R$ reaches equilibrium with the gas phase. If we apply the lower limit diffusion coefficient to this relationship, $2x10^{-14}$ cm^2/s, a subsurface zone > 200 Å is deduced under the "optimum" PECVD growth. The deep traps of capture rate α_r in this zone become saturated if $R<(D_H C_{do} \alpha_r)^{1/2}$.

Our results can be compared with the very recent studies of Branz et al. [18] and Jackson and Tsai [19] which focus on SIMS measurements and suggest trap-controlled diffusion. For example, Branz et al. propose a diffusion coefficient of $3x10^{-8}$ cm^2/s for H in the transport level and a mean free path of 450 Å before a deep-trapping event occurs. These results are consistent with our observations. Equations (10-11), developed independently here, are the same as those of Jackson and Tsai [see their Eqs. (2-3)]. In our work, however, we focus on the direct kinetic information in C_r. In contrast Jackson and Tsai, out of necessity, must focus on the spatial dependence. A detailed comparison of the results of our study with the latter is beyond the scope of the present report.

3.6 Effect of Sample Temperature on the Eqilibration of the Chemical Potential

We have explored the effect of a-Si:H temperature on the equilibration processes described in Parts 3.4 and 3.5. In all cases the starting a-Si:H film was deposited onto c-Si at 240°C under optimum conditions, and the H-treatments were performed after cooling to either 200°C or 160°C. All H-treatment conditions were identical: 28 W filament power and 8 mTorr pressure. After about an hour, the optical spectra in all cases saturated, exhibiting no further changes with continued H-treatment. Figure 16 shows the results of a linear regression of the final saturated (ψ,Δ) spectra at 160°C and 200°C. Also included for comparison are the results for the 240°C H-treatment of Fig. 9. We found that for the 160°C and 200°C hydrogenation, it was necessary to split the film into a multilayer structure with different volume fractions for the Si-H reacted component in each layer. Thus, the data in Fig. 16 can be viewed as step-wise approximations to depth profiles in the Si-H component volume fraction above the level that was originally present in the film. The behavior of the samples at the lower temperatures differs from that at 240°C, since the latter does not exhibit a strong spatially varying profile at saturation.

Because of their stability with time (i.e. such results were obtained at saturation), it is clear

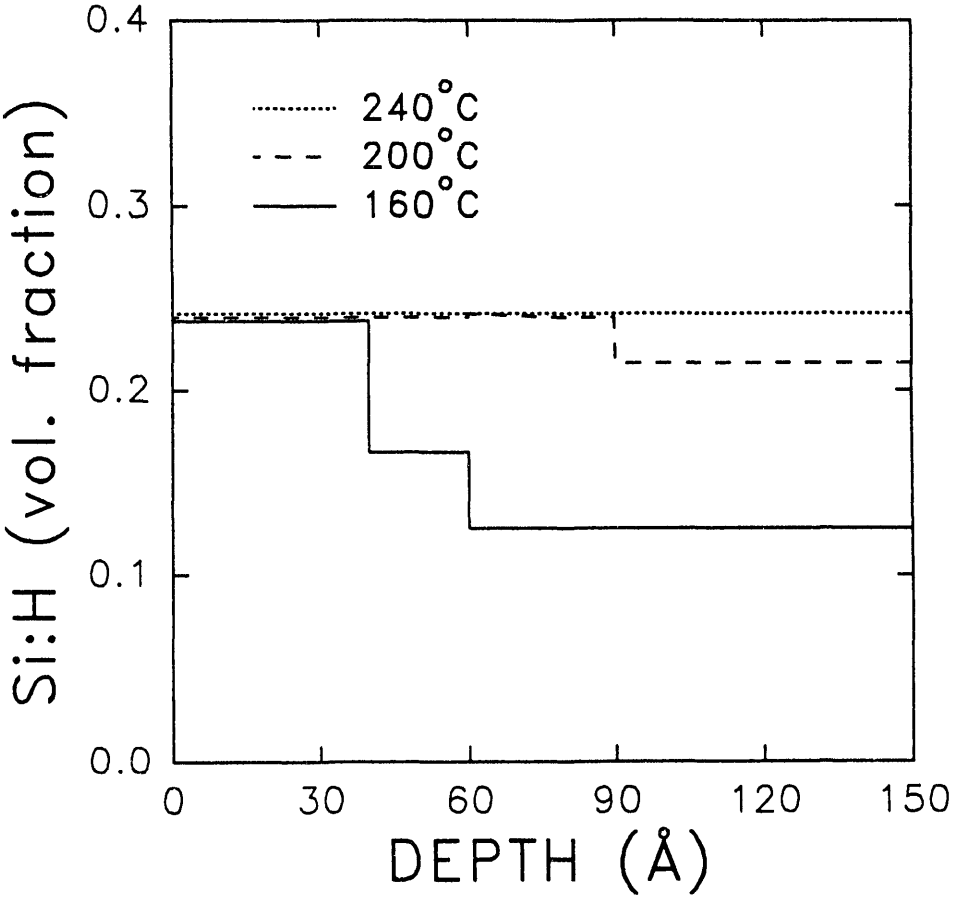

Fig. 16 Experimental depth profiles of the Si-H component volume fraction obtained from real time ellipsometric spectra collected after one hour exposures of a-Si:H to atomic H. In three separate experiments the sample temperatures were held at 160°C, 200°C, and 240°C. The profiles shown here were found to be stable under prolonged atomic H exposures. At the highest temperature of 240°C, a spatially varying profile was not needed to fit the experimental spectra closely in the top 200 Å.

that the profiles at 160°C and 200°C are not conventional diffusion profiles, and one would need to solve Eqs. (10) and (11) in the general situation where diffusion and reaction compete on the same time scale as has been done in Ref. 19. An intuitive interpretation of Fig. 16 would suggest that chemical equilibration with the gas phase occurs only in the top ~50 Å at 160°C, and the chemical potential then falls off with distance into the bulk a-Si:H. Similarly at 200°C, chemical equilibration has occurred fully only in the top ~100 Å of the film. The fact that the volume fraction of the reacted Si-H component reaches a stabilized value of 0.24 independent of substrate temperature suggests that the same relaxed structure is achieved as controlled by the gas phase chemical potential, and no further Si-Si bonds are broken even with continued exposure.

Figure 17 shows the best fit single rate coefficient deduced from the Si-H component volume fraction as a function time at the three different temperatures. These results were obtained from the reaction kinetics of the subsurface a-Si:H concentrating on the full energy range (top 500 Å of the film). The error bars include three sources: (1) uncertainties in the fit to the reaction law, (2) smaller populations Si-H sites with different rate coefficients that were neglected in the analysis, and (3) possible depth dependence in the reaction coefficient that was also neglected. First, the results of Fig. 17 imply that $\alpha=4\pi r_c D_d C_{do} \exp(-\delta E_r/kT)$ is nearly constant with temperature. Because D_d is expected to increase with temperature, if at all, then the error bars in Fig. 17 imply that $\delta E_r<0.1$ eV, and there is no significant barrier to deep-trapping. This also indicates that D_d is also weakly temperature dependent over the 160°C-240°C range. This result is consistent with the conclusions of Branz et al. [18] who first suggested that the free H diffusion coefficient is nearly temperature independent.

3.7 Effects of Surface Bonding on Equilibration: The Oxide Diffusion Barrier on a-Si:H

Figure 18 presents the time evolution of the deep-trapped Si-H component determined by linear regression analysis of real time SE data collected during H-exposure of two different a-Si:H surfaces. In both cases, the H-treatment conditions were the same: 40 W filament power, 4 mTorr H_2 pressure, and 250°C sample temperature. For the open points, the H-treatment was performed immediately after a-Si:H deposition, and the results fit Eq. (7) and exhibit behavior consistent with that presented previously (Fig. 15). For the solid points, the a-Si:H was exposed to the laboratory atmosphere just after deposition and prior to the H-treatment. The a-Si:H was held at 250°C during exposure to air, and because the Si-H_n layer on the a-Si:H surface is unstable at this temperature, a thin native oxide layer is formed. An estimate based on real time SE indicates that the oxide is no more than a few monolayers in thickness (<10 Å). Figure 18 shows dramatically that the oxidized surface exhibits no significant bulk conversion of Si-Si bonds to Si-H bonds. In fact the effect detected (<0.01 volume fraction increase in Si-H component after 30 min), is so small that it is difficult to ensure that it represents true bulk

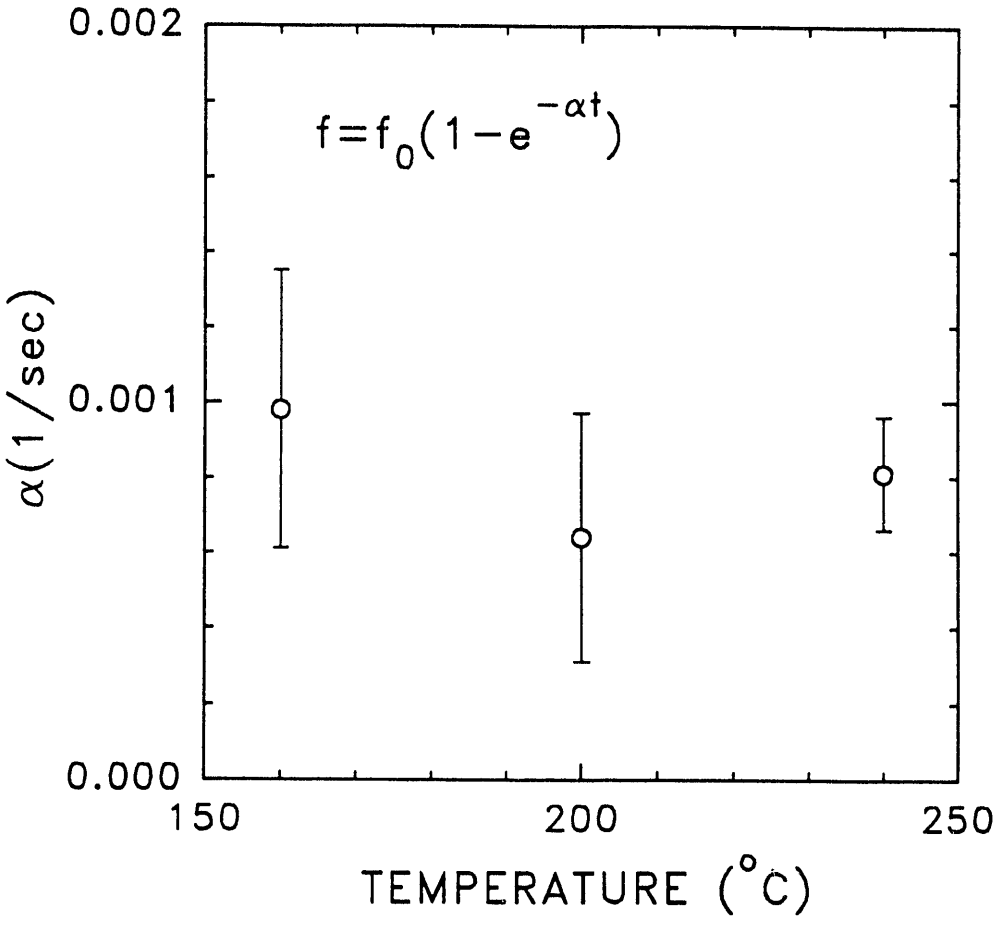

Fig. 17 Rate coefficients for the deepest layers of the profiles in Fig. 16 deduced from real time ellipsometric spectra collected during atomic H exposure of a-Si:H at three different temperatures. To obtain these values, data such as those in Fig. 15 were fit to linear behavior. See text for explanation of confidence limits.

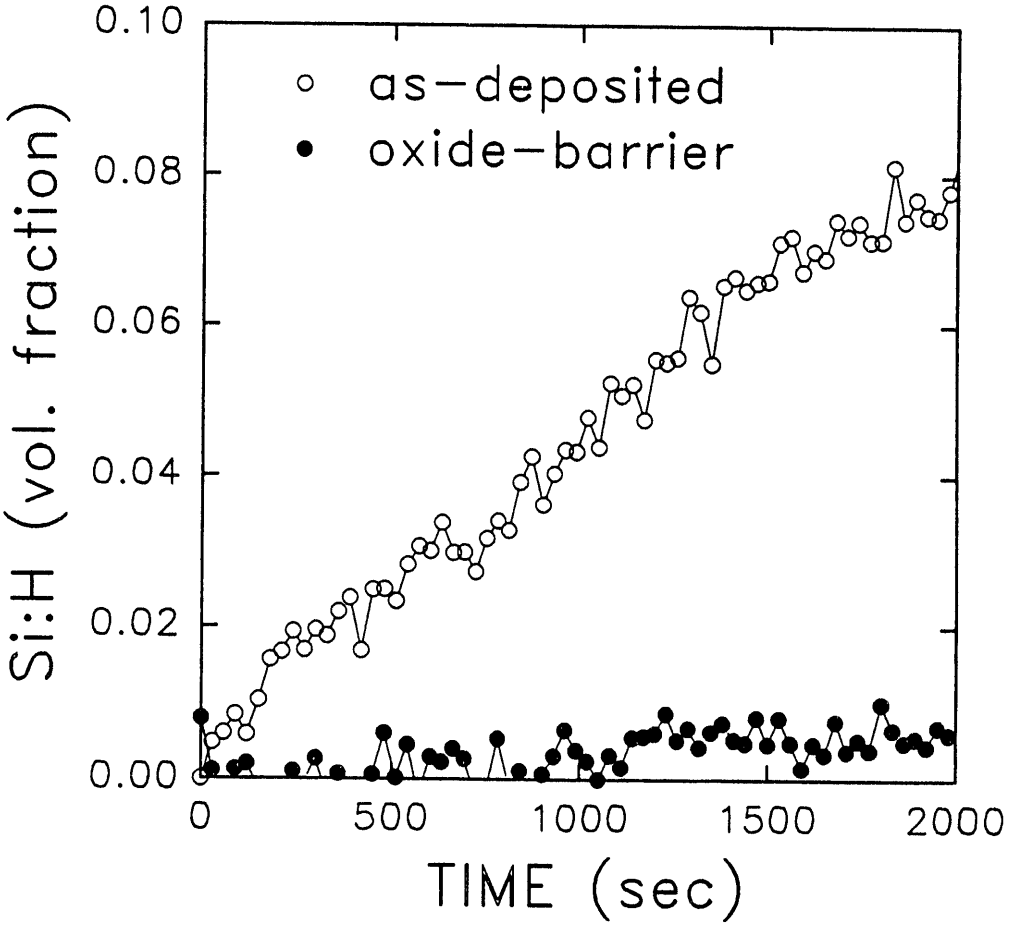

Fig. 18 Volume fraction of Si-H component determined from real time ellipsometric spectra during atomic H exposure of optimum PECVD a-Si:H at a temperature of 250°C. For the open points, the H-treatment was performed immediately after deposition; for the solid points, the sample was exposed to the ambient immediately after deposition, and prior to the H-treatment.

conversion to Si-H.

Thus, the results show clearly that a near-monolayer thickness of native oxide on a-Si:H provides a very effective barrier to free H which prevents equilibration of the gas phase and solid chemical potentials. With the diffusion of H prevented, the reaction of H with Si-Si bonds according to Eqs. (8-9) is prevented as well. Thus, we suggest that the first step in the diffusion process is as follows:

$$H(g) + (H_nSi\text{-}Si_{4-n})(s) \rightarrow H_nSi\text{-}H\text{-}SiSi_{3-n}(s). \quad (13)$$

where n=1 or 2. (If n=3, then etching would occur.) Here H switches from a terminating bond site at the surface to a bridge-bonded or bond-centered site below the surface, which then permits further diffusion into the bulk. When the -SiH bonds on the surface are replaced by stronger -SiO bonds, the H hopping mechanism is blocked. If H were to enter the network as an interstitial with its electron cloud intact, it seems that the nature and strength of the surface bonding would exert much less influence over the diffusion behavior.

In addition to the fundamental insights that the results of Fig. 18 provide, the practical implications are of great importance. First it suggests that any chemical equilibrium approaches to materials processing (such as that used here) must be performed in situ. Once a native oxide layer forms on the surface or anywhere else in the structure, it acts as an effective barrier to equilibration through the depth of the film. This also means that the oxides at the interface to the substrate act as a barrier to trap diffusing H within the film. This is important for diffusion/reaction equilibration processes in very thin films since the boundary conditions are different than those leading to Eq. (6). The implications of our results for interpreting H-evolution are not yet fully clear. We expect that an oxide layer would also serve as a barrier for out-diffusion of hydrogen, and all thermal H evolution studies in the literature are performed on materials with surface oxides.

3.8 Stability of the Elevated Chemical Potential in Thin Film a-Si:H

It is important both from a fundamental and practical standpoint to characterize the stability of the Si-H bonding configurations that have been established in the presence of the elevated chemical potential. Figure 19 shows the evolution of the excess Si-H component volume fraction (solid points) and surface morphology (open points) as a function of time after extinguishing the filament and terminating the atomic H exposure. To begin this experiment, a 30 min H-treatment of a 4000 Å thick a-Si:H film, prepared under optimum conditions, led to a 11 vol.% increase in the Si-H bond component. However, Fig. 19 reveals that more than 1 vol.% of this material reverts to the original bonding when the gas phase chemical potential is

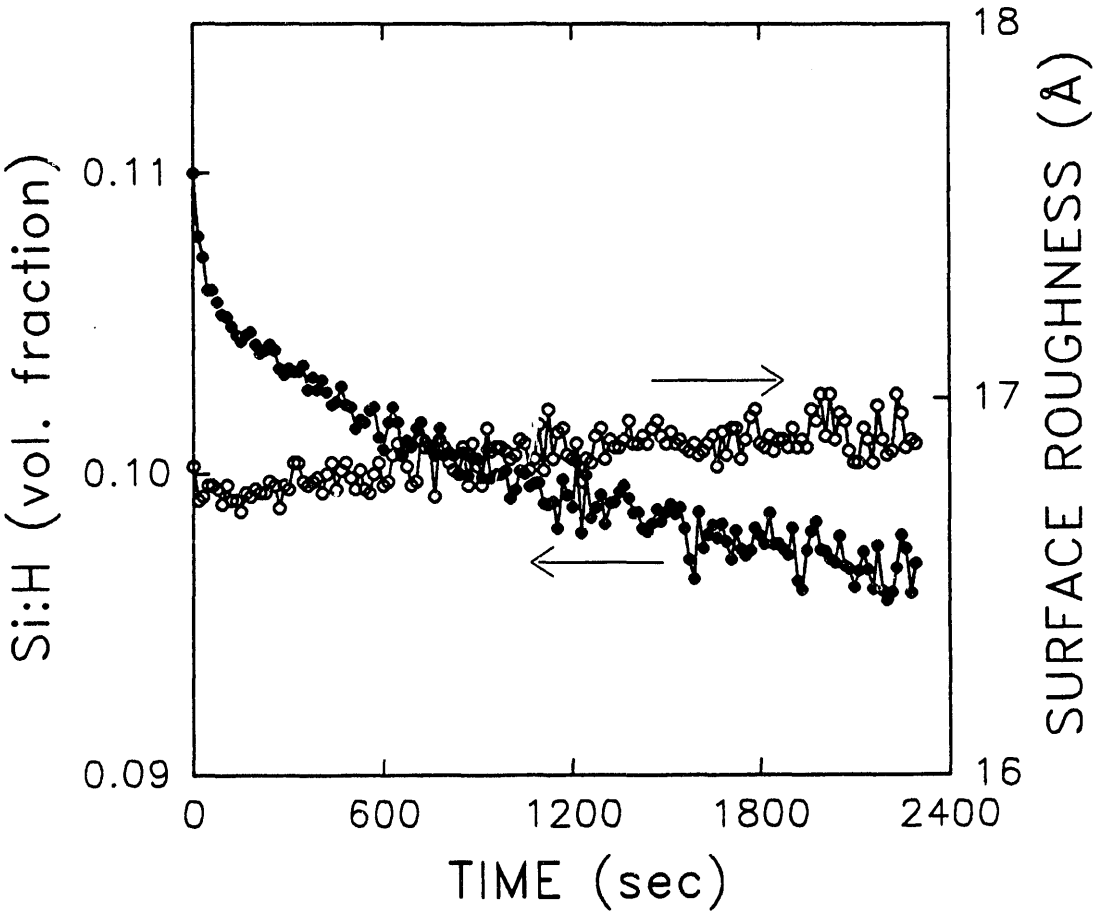

Fig. 19 Volume fraction of bulk Si-H component in H-treated a-Si:H, determined as a function of time after extinguishing the atomic H filament source at t=0, but maintaining the sample temperature at the value used in the treatment, 240°C. Prior to extinguishing the filament, the 4000 Å thick a-Si:H was exposed to the atomic H environment for 30 min, generating ~11 vol.% excess Si-H component. The reduction in the component fraction after 30 min of annealing is ~1 vol.%. The constant surface roughness value within ±0.1 Å, demonstrates a contant Δ spectrum in the real time SE experiment, and thus emission rate-limited conversion of Si-H volume throughout (at least) the top 500 Å of the film at 240°C. The measurements provide information on bonding changes with an emphasis on the top 200 Å of the film.

returned to the vacuum level. A 24 hour anneal for the sample of Fig. 19 suggests that 85% of the Si-Si bonds broken upon H-treatment are irreversibly broken. It is important to note that we do not detect any similar change in bonding after preparation of a-Si:H when the SiH_4 plasma is extinguished. Such an effect undoubtedly occurs, however, but the number of bonds participating is probably very low.

We find that the reverse process of Si-Si bond formation from Si-H bonds is "reaction-limited" to a depth of 500 Å as observed by a nearly time-independent Δ spectrum. It appears from the SE, then, that the profiles in the Si-H component fraction remain constant at least to a penetration depth of 200 Å. With the removal of the free H source (C_{do}=0) that establishes the deep-trapping kinetics of Eq. (11), the only term left is H emission, which was neglected in Eq. (11). Thus, we have:

$$\partial C_r/\partial t = -\alpha_e C_r = -C_r \alpha_{oe} \exp(-\Delta E/kT) \qquad (14)$$

where α_e is the emission rate, α_{oe} is the attempt frequency for emission, and ΔE is the trap depth. The range of trap depths probed in the entire experiment of Fig. 19 is 1.3 eV to 1.9 eV (observation times from 1 s to 1 day; longer time data not shown).

Because 85% of the H remains in the film after a 24 hour anneal, the majority of the deep-trapped H observed optically is characterized by a rate coefficient for emission of $<5\times10^{-7}$ s^{-1}, meaning it is trapped more than 1.95 eV below the transport level. Over the observed time scale, the dominant range of rate coefficients is $(0.4\text{-}4)\times10^{-3}$ s^{-1} corresponding to trap depths of 1.5-1.6 eV. These traps contains about 15% of the total incorporated H. Because 85% of the trapped H species have emission rates a few orders of magnitude lower than the capture rate, then it is reasonable at this point to neglect the emission terms as we have done in Eqs. (10) and (11). The importance of this work is that it identifies a number of H-trapping sites based on the energy differences. The trap with 15% of the H may be the one responsible for the observed H diffusion behavior commonly reported.

One important feature of this partial reversion is its potential impact on the ex situ characteristics of the thicker films prepared by alternating growth and H-treatment, as highlighted earlier in Section 3.1. Further discussion on this point appears in Sect. 3.11.

3.9 Etching of a-Si:H by Hot Filament-Generated Hydrogen

A tendency toward etching of a-Si:H thin films during the H-treatment can be stimulated by varying a number of parameters. It appears that if H does not efficiently move from the near-surface region of the film either back into the gas phase or into the bulk of the film, and the

concentration of broken Si-Si bonds reaches a critical value, etching will occur. Another way of viewing this is that if the chemical potential of H near the surface is raised too high, the Si at the surface will undergo massive structural changes [8].

Each of the following effects has been observed experimentally. (1) An increase in the filament power beyond a critical value leads to etching. This simply increases the gas phase H chemical potential at the surface. (2) H-exposure of the a-Si:H at reduced temperatures enhances etching. A larger number of the traps in the top few monolayers (not detected in Fig. 16) may become deep traps leading to a larger volume fraction of Si-H in the very near surface region which can destabilize the network. (3) Thin a-Si:H films are more susceptible to etching than thick films. In thick films, the bulk material serves as a sink for free and shallow-trapped H (which converts to Si-H bonds at the rate of 10^{-3} s^{-1}). In very thin films, the concentration of diffusive H increases to capacity very quickly, and presumably the driving force for diffusion, the gradient in the chemical potential, is reduced. Such an effect also leads to extensive trapping of H in the near surface region.

Figure 20 shows an example of the use of real time ellipsometry to characterize the etching and bulk Si-Si bond conversion for a 150 Å thick a-Si:H film during exposure to the heated filament under different conditions. At 20 W with a rear-mounted filament (r), any etching over the 10 min time of observation is less than a single monolayer. When the power is increased to 35 W, a slow layer-by-layer etching process at an average rate of 0.01 Å/s is detected. Using the same power, but applied to a front-mounted filament (f) with direct line of sight to the sample, rapid etching is observed which appears to accelerate in conjunction with increased bulk Si-Si bond conversion.

Figure 21 shows the imaginary part of the dielectric function for a 17 Å thick film deduced in an analysis of real time SE data collected during etching (in the terminal stages). Also shown for comparison are the corresponding results for a 21 Å a-Si:H film obtained during the optimum PECVD process. Two features are immediately apparent: (1) the steeply rising absorption onset is characteristic of pure crystalline Si, and (2) the Si atom density in the etched film is significantly higher than that in the nucleating a-Si:H film. From (1), we conclude that under etching conditions the chemical potential in the near surface region is sufficiently high so that massive restructuring to a higher degree of order occurs. Furthermore from (2), we conclude that the etching is relatively uniform with the formation of densely packed crystalline domains on the surface. In this way, ultrathin, dense, single-phase μc-Si:H films can be prepared. Similar densities of μc-Si:H prepared by PECVD of SiH_4:H_2 mixtures occur only after a hundred or more Ångstroms. Thus, we suggest that an improved preparation technique [20] for such materials would involve alternating a-Si:H growth with hot-filament H-treatments, and growing films at ~15 Å per cycle.

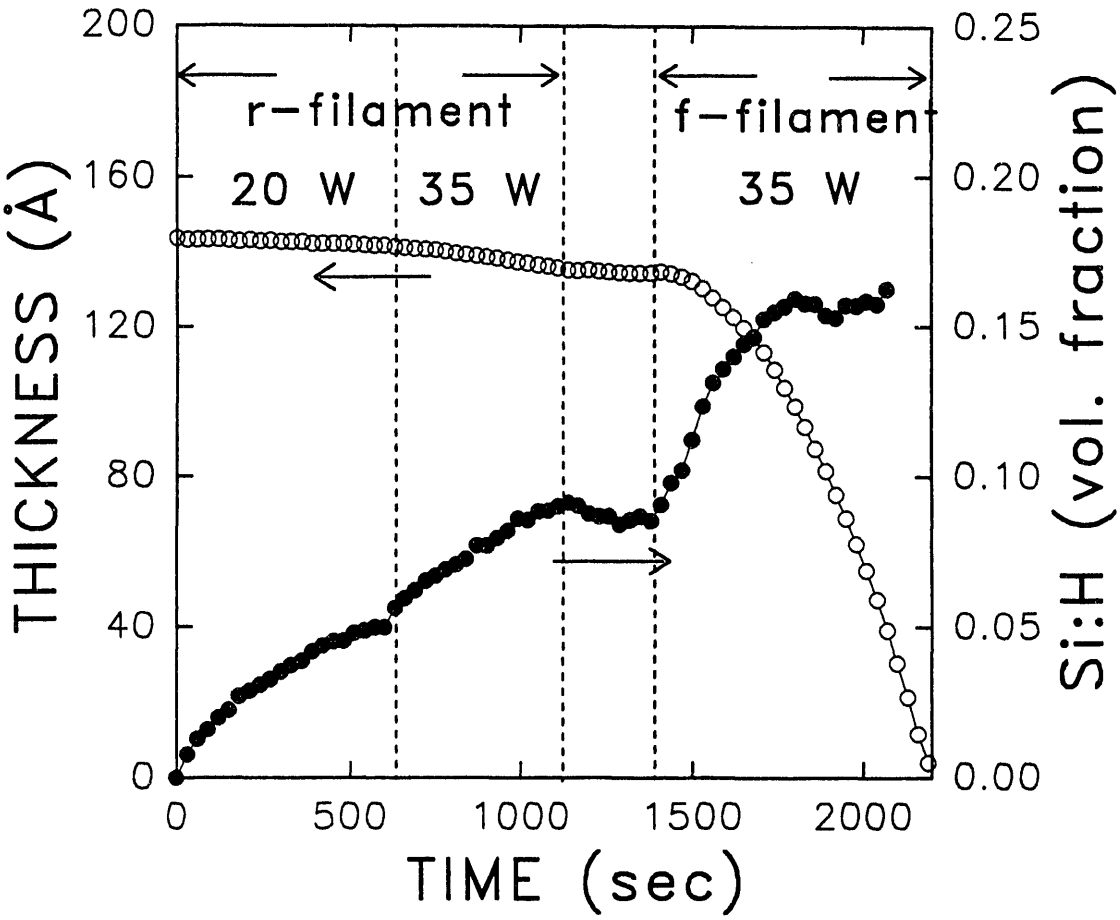

Fig. 20 Volume fraction of Si-H component, and bulk film thickness as a function of time during H-treatment of ~150 Å thick optimum PECVD a-Si:H. The values at the top denote the power applied to the heated filament. Initially a rear (r) filament was used without direct line-of-sight to the sample; later a front (f) filament was ignited under the same conditions. The front-filament configuration at 35 W leads to rapid etching owing to direct line of sight to the sample surface.

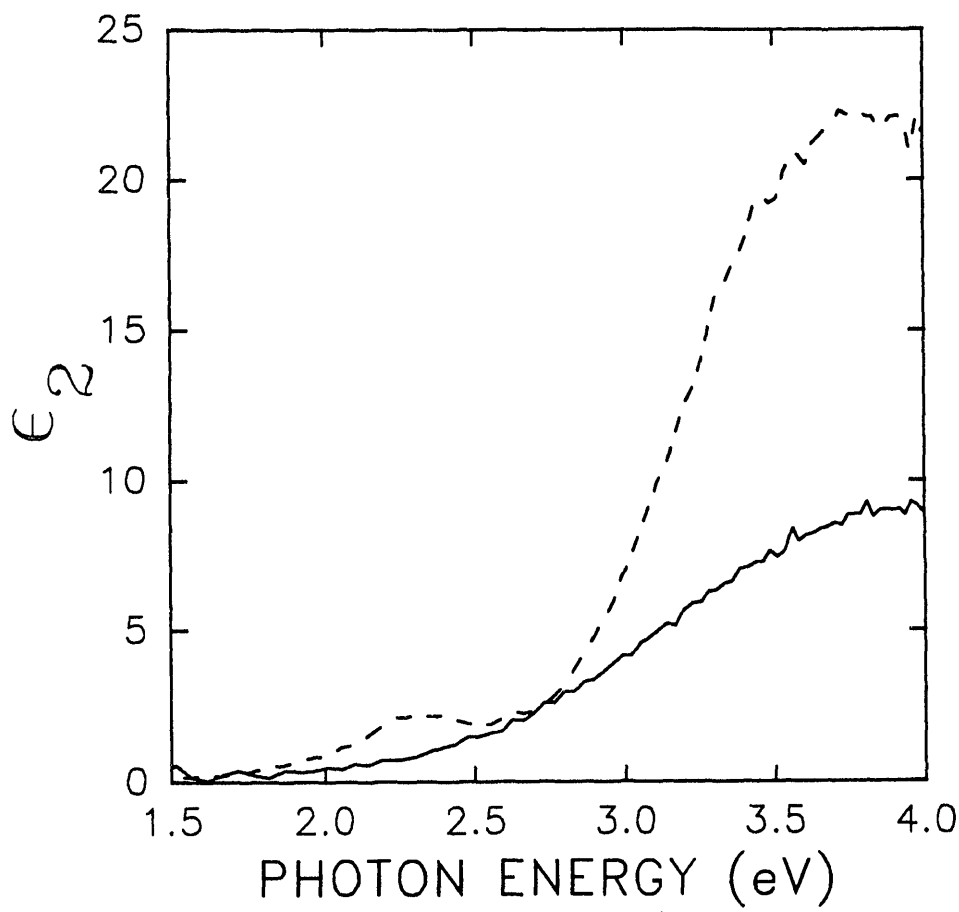

Fig. 21 Imaginary part of the dielectric function of a 17 Å thin film remaining on the substrate surface in the terminal stages of etching (as in Fig. 20) as determined by real time SE (broken line). Corresponding results were obtained for optimum PECVD a-Si:H in the initial stages of growth when the film consists of clusters 21 Å thick (solid line). In both cases the substrate was chromium. The steeply rising ε_2 value indicates that the film measured during etching is well-ordered c-Si.

3.10 Studies of Unhydrogenated Amorphous Silicon Prepared by Sputtering Comparsion of Si-Si Bonding Distributions

In contrast to previous indications in the literature [9], here we briefly note that all the same phenomena reported in Sections 3.4-3.9 have also been observed for pure a-Si films prepared by sputtering. This suggests that these phenomena, including fast diffusion and Si-Si bond breaking by excess H, are not influenced significantly by the presence of H or dangling bonds in the starting structure.

There are some interesting differences between the response of PECVD a-Si:H and sputtered a-Si, however. For sputtered a-Si, the Si-H bond transient corresponding to Fig. 15 cannot be fit as closely with a single exponential decay. A much closer fit is obtained using two exponentials with distinct rate coefficients that differ by an order of magnitude. The volume fraction of Si-H associated with the faster capture rate is found to be a factor of three lower than that of the slower capture rate, and the former appears to correspond to roughly 1 at.% of the total bonds in the network. If the corresponding double exponential fit is performed on the PECVD transient of Fig. 15, then a similar division between two sets of bonds is obtained, and again the difference in capture rates is one order of magnitude. However, in this case the volume fraction associated with the high capture rate sites is more than a factor of 10 lower than that of the low capture rate sites and corresponds to ~0.3 at.% of the bonds in the network. Recently, the quantity of Si-H in the high capture rate sites has been found to scale with void volume fraction, presumably because of a higher value of D_d, and hence a higher capture cross-section for sites located along void channels.

Finally, we note that under identical filament conditions it is possible to break a larger number of Si-Si bonds in sputtered a-Si before the etching threshold is reached. This is a simple consequence of the fact that the original material has no hydrogen, and more hydrogen is needed to raise the chemical potential to its maximum possible while maintaining an amorphous structure.

3.11 Ex Situ Characterization of Thick Modified Materials Prepared by Alternating Growth and H-Treatments

The real time SE studies can be performed even on ultrathin films. However, to characterize other properties of the H-treated PECVD materials, we needed to generate thicker films in such a way as to incorporate the excess H as uniformly as possible, maintaining a constant chemical potential throughout the film thickness. Furthermore we needed to ensure that the chemical potential was not raised too high at any stage of the growth process in order to avoid microcrystal formation on the surface. The real time SE study described above guided our

selection of the appropriate processing parameters.

In the first set of depositions, we alternated 850 Å of optimum a-Si:H growth (10 min) with 20 min H exposure. The H exposures were performed with a 35 W filament power and 8 mTorr H_2 pressure. From the SIMS study described above, it was clear that uniformity in the Si-H component depth profile was obtained to ~200 Å, and the H-content falls by a factor of two by 300 Å. The 10/20 min duty cycle when combined with a long time anneal is expected to allow the entire sample to equilibrate. As noted below, lower quantities of excess H can be incorporated (resulting in a lower chemical potential in the film) either by reducing the H-treatment time or the filament power during treatment. In our initial studies the interest was in higher H-content materials.

Table I shows the results of an infrared absorption study of a film prepared with 10 cycles of 10/20 min growth/treatment using a substrate temperature of 220°C. The experimental data corresponding to these parameters appear in Fig. 2. As a result of the H-treatments, we are able to increase the H content of the film from 9 at.% to 13 at.%, as measured from the wagging mode along with literature oscillator strengths [21]. A corresponding estimate from the stretching mode absorption is 3 at.%. Of the total excess H incorporated, 80% appears in the 2000 cm^{-1} and the remainder in the 2100 cm^{-1} mode, as noted earlier. This behavior is typical of numerous films prepared by cycling growth and H-treatment under these filament conditions.

Table II shows the accumulated results of property measurements on the material prepared in the deposition of Table I and Figs. 2 and 3. Here we will briefly comment on the important features of the data, which are typical of all materials H-treated under these filament conditions. The optical gap increases by about 0.04 eV. The $\mu\tau$-product for electrons tends to be higher for the H-treated materials in the annealed state in comparison with the untreated materials; however the degradation of $\mu\tau$ is such the differences tend to be reduced in the light-soaked state. Although there appears to be a slight improvement in the Urbach tail parameter for the 10/20 cycle deposition (as noted earlier; see Fig. 3), this effect is within our experimental error (±0.01 eV), and we conclude that the gap widens relatively rigidly with H excess incorporation. Finally, we note that the integrated absorption in excess of the Urbach tail, which we ascribe to dangling bonds in the usual fashion, is somewhat lower in the H-treated samples. However, no significant change in the stability under light soaking is observed.

One important observation noted earlier, is the ability of the electronic structure to reach equilibrium under H-treatment without the generation of additional dangling bonds. It is clear that the H chemical potential in the cycled materials has been raised; however it is not clear that this has led to any preferential conversion of weak Si-Si bonds to Si-H bonds. (Earlier it was stated that the Urbach tail slope is sensitive to such a preference only when it becomes greater than 2; i.e. twice as many weak bonds broken as strong bonds.) It must be a manifestation of the fine balance of chemical equilibrium that a disruption of $2x10^{21}$ cm^{-3} Si-Si bonds in the

Table I A summary of the analysis of the infrared transmission spectra of Fig. 2 for two PECVD a-Si:H films 0.85 μm thick, deposited on c-Si at a substrate temperature of 220°C. One film was prepared by continuous PECVD without any H-treatment. The other film was prepared by alternating 10 min of PECVD growth (~850 Å) with 20 min H-treatment for 10 cycles. Literature oscillator strengths were used to relate integrated absorption to hydrogen content independently for both the wagging and stretching mode regions. Based on these results, we estimate that the H-treatments led to 3.5-4 at.% additional H-content.

Continuously Grown		Intermittently Grown/Hydrogenated	
Peak Position K_i (cm^{-1})	Hydrogen Content $C_H(K_i)$ (atomic %)	Peak Position K_i (cm^{-1})	Hydrogen Content $C_H(K_i)$ (atomic %)
629.6	9.20	630.9	13.02
1996.0	8.58	2002.6	11.09
2097.0	1.31	2097.1	1.79

Table II Optoelectronic properties of samples prepared by alternating 10 min of a-Si:H film growth with 20 min of H-treatment at 35 W filament power. Results for two untreated companion samples "No H" are also provided. Measurements include, from top to bottom: Tauc gap, H-content from ir wagging mode, conductivity activation energy, conductivity prefactor, 25°C conductivity in annealed and light soaked states, exponent in the generation rate (G) dependence of the photoconductivity in the two states, mobility-lifetime product for electrons (G=10^{16} and 10^{19} $cm^{-3}s^{-1}$) in annealed (AN) and light-soaked (LS) states , Urbach slope, and defect density estimated by integrating the sub-gap absorption in excess of the Urbach tail.

Substrate T			T_s=220°C	
Film Status			No H	H(10/20)
E_g (eV)			1.73	1.77
C_H (at. %)			9.2	13.0
E_a (eV)			0.65	0.69
σ_0 ($\Omega^{-1}cm^{-1}$)			180.5	361.7
σ_D ($\Omega^{-1}cm^{-1}$)	Annealed State		$2.45x10^{-9}$	$9.25x10^{-9}$
	AM1, 20H Soak		$2.26x10^{-10}$	$9.69x10^{-9}$
γ	Annealed State		0.76	0.83
	AM1, 20H Soak		0.82	0.83
$\mu\tau$	AN	G=10^{16}	5.1e-5	6.7e-5
		G=10^{19}	1.0e-5	1.8e-5
	LS	G=10^{16}	9.4e-7	1.1e-6
		G=10^{19}	3.0e-7	3.1e-7
E_0 (meV)	Annealed State		49	47
	AM1, 20H Soak		50	48
N_{DB} (cm^{-3})	Annealed State		$7.0x10^{15}$	$5.1x10^{15}$
	AM1, 20H Soak			
	AM1, 200H soak		$2.0x10^{16}$	$2.03x10^{16}$

network does not alter processes on the scale of 10^{16} cm^{-3} defects.

When specific microscopic models are considered, however, our results are more difficult to understand. For example in the traditional bond-breaking/H-diffusion models for light induced defects that have been developed over the years, the rate of defect generation is predicted to be proportional to the H concentration [22]. In one model, this may arise from the fact that H-diffusion separates the two dangling bonds generated at a weak Si-Si bond site by a band tail carrier, and this occurs more readily at high H content. In another case, excess carriers increase the rate of release of H which can then diffuse and break weak Si-Si bonds, and this effect also is enhanced at high H content. Our results do not support such models since we have increased the H-content by nearly 50%, but observe similar generation rates for light-induced defects.

It is possible that we have managed to reduce the density of susceptible weak bond sites to balance the H-content increase, but if this has happened, it is not visible in the electronic density of states. Another possibility is that the H incorporated in the treatment is bonded in clustered sites that neither contribute to the Staebler Wronski effect as light-induced defects, nor are sufficiently mobile to separate any light-induced dangling bonds. This makes sense considering the large deep-trapping energies for the H incorporated during treatment (>1.9 eV). In fact, clustered sites are expected to have a relatively large binding energies [19].

We have proceeded to assess the possibility that in the first series of samples, an improvement provided by stabilization of the network upon H-treatment may be offset by the detrimental effects of the ~4 at.% excess H incorporation. As a result, we studied a second series of H-treated a-Si:H samples and untreated control samples. For the treated samples in this series, a lower power of 12 W was applied to the filament, and 16 total cycles consisting of 5/10 min growth/H-treatment followed by an anneal provided equilibrated films 0.65 μm in thickness.

The properties of two representative samples of this second series with T_s=220°C are shown in Table III. For both sample pairs in Tables II and III, the control was prepared immediately before or after its H-treated companion sample in the series. In this way, we minimize irreproducibilities unrelated to the H-treatment. The difference between the two untreated control samples in Tables II and III can be related to problems typically encountered with single chamber preparation. The samples in Table III were prepared after a long series of microcrystalline Si depositions, and the resulting positive effect of H-plasma cleaning of the internal chamber components led to improved properties for these samples. This can be seen most clearly from the factor of ~three lower defect density in the a nealed state in Table III ($2x10^{15}$ cm^{-3}) in comparison to the results of Table II ($7x10^{15}$ cm^{-3}). By drawing on the results from a number of samples of different substrate temperatures from 220°C-250°C, we avoid erroneous conclusions based on random run-to-run irreproducibilities.

Infrared transmittance measurements in the wagging and stretching mode regions of the thick treated film (0.65 μm) of Table III, as well as real time SE studies of single cycle films

Table III Optoelectronic properties of samples prepared by alternating 5 min of a-Si:H film growth with 10 min of H-treatment at 12 W filament power. Results for an untreated companion sample are also provided. Measurements include, from top to bottom: Tauc gap, H-content from the ir wagging mode (W), and independently-determined contributions from 2000 cm^{-1} (S1) and 2090 cm^{-1} (S2) stretching modes, conductivity activation energy, conductivity prefactor, 25°C conductivity in annealed and fully light-soaked states, exponent in the generation rate (G) dependence of the photoconductivity in the two states, mobility-lifetime product for electrons ($G=10^{16}$ and 10^{19} $cm^{-3}s^{-1}$), Urbach tail slope, and defect density estimated by integrating the sub-gap absorption in excess of the Urbach tail.

Film Status			Untreated	H-treated
E_g (eV)			1.76	1.78
C_{II} (at. %) (W)			9.20	11.57
C_{II} (at. %) (S1)			8.58	9.81
C_{II} (at. %) (S2)			1.31	1.69
E_a (eV)			0.90	0.99
σ_0 ($\Omega^{-1}cm^{-1}$)			$2.3x10^{5}$	$5.3x10^{5}$
σ_D ($\Omega^{-1}cm^{-1}$)	Annealed		$1.4x10^{-10}$	$1.5x10^{-11}$
	Light-soaked		$5.5x10^{-11}$	$1.5x10^{-11}$
γ	Annealed		0.96	1.00
	Light-soaked		0.81	0.85
$\mu\tau$ (cm^2V^{-1})	Annealed	$G=10^{16}$	$1.5x10^{-6}$	$1.7x10^{-6}$
		$G=10^{19}$	$1.1x10^{-6}$	$1.7x10^{-6}$
	Light-soaked	$G=10^{16}$	$6.7x10^{-7}$	$4.6x10^{-7}$
		$G=10^{19}$	$1.3x10^{-7}$	$1.4x10^{-7}$
E_0 (meV)	Annealed		47	50
	Light-soaked		51	52
N_{DB} (cm^{-3})	Annealed		$2.04x10^{15}$	$1.72x10^{15}$
	Light-soaked		$2.20x10^{16}$	$1.37x10^{16}$

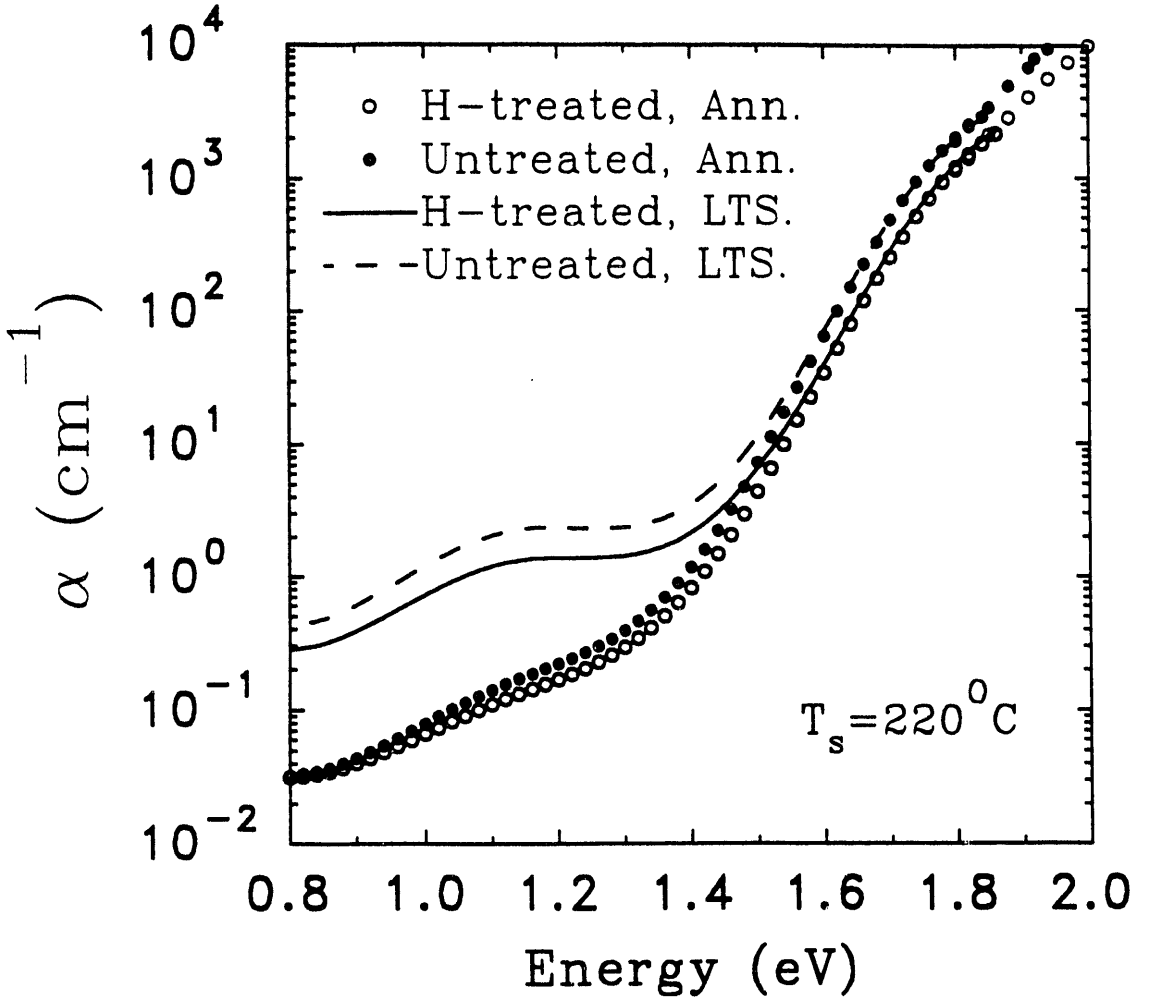

Fig. 22 Absorption spectra obtained from 0.8 to 2.0 eV using a combination of dual beam photoconductivity, transmittance, and reflectance measurements for H-treated and untreated PECVD a-Si:H in fully light-soaked (LTS) and annealed (Ann.) states. In this case the treated sample was prepared by alternating 5 min growth with 10 min H-treatment. For the H-treatment, the filament power was set at 12 W.

(400 Å) under the same filament conditions, both suggest that ~1.5-2 at.% additional H is incorporated as a result of the low power H-treatment, at least a factor of two smaller than the first series. This results in a larger optical gap by ~0.02 eV for the treated film in comparsion with the untreated film.

Figure 22 highlights the results of subgap and near-band edge absorption measurements for the treated and control samples of Table III in the annealed and the fully light-soaked states (i.e. 50 hrs. at 10 x AM 1 for the latter). The interesting observation to be noted here is that the increase in midgap defect density with light-soaking is 40% lower for the H-treated sample in comparison to the untreated sample. In fact, the low defect density for the H-treated sample in Table III appears to be unique to the H-treatment process and comparable results have never been obtained for other (untreated) a-Si:H materials optimized for defect density in the annealed state. Although the improvement in stability is not overwhelming, it suggests that further studies of materials prepared as a function of the H-treatment conditions are warranted in order to minimize the defect density in the light-soaked state. The importance of the work lies in the fact that it is straightforward to "retrofit" a heatable filament into existing PECVD reactors for bulk film and interface modification.

Thus, we suggest that the null results for the first series of samples (see Table II) may be related to excess H incorporated in the higher power H-treatment process. Apparently for the second series of samples, the stabilization of light-induced defects overcomes the detrimental effect of H which is weaker because of the lower excess H-content. A previous approach to higher stability has in fact emphasized a reduction in H content to ~3 at.% as a key factor [23]. Recently, however, more stable films have been prepared with H contents equivalent to the conventional PECVD (~10 at.%) with higher substrate temperature as a key [24].

There are two possible origins for the improved stability of our second series of H-treated films. First, the fraction of weak Si-Si bonds may be smaller in the H-treated materials. Second, the H rearrangements by which chemical equilibrium is reached may lead to more stable H configurations. The first possibility seems not to be supported since the Urbach tail in the H-treated sample in Table III appears slightly broader (see Fig. 22). At this point, however, it is not clear whether the additional tail states are associated with the Si-Si network or are stable H- or impurity-related defects. In any event, further characterization and optimization of these hydrogen-equilibrated films must be made before more definitive models can be proposed.

4. Microstructural Evolution a-Si:H Nucleation and Coalescence: A Final Word

We will conclude with a brief description of the results obtained in the second component of our research: the structural evolution of a-Si:H during nucleation and growth. New quantitative information is now available with the increase in sophistication from real time single

wavelength ellipsometry to real time spectroscopic ellipsometry (SE). In fact, we have developed our real time SE to operate at 64 ms acquisition and repetition times, faster than any previous studies with a single wavelength instrument, and still maintaining monolayer resolution. Such capabilities now allow us to characterize film growth at rates as high as 50 Å/s, permitting studies of the microstructural evolution at high rf plasma power densities as reported below.

We have found that a two-layer optical model with three free microstructural parameters at each time characterizes the dynamic processes of thin film nucleation and coalescence [25]. Such a model cannot be verified on the basis of single wavelength ellipsometry, which returns two parameters [(ψ,Δ)] at any given time. A real time spectroscopic capability (which in our case returns more than one-hundred experimental parameters) is needed to verify the validity of the model and deduce the three parameters. These parameters are as follows: (1) d_s, the thickness of a surface layer of low bond-packing density; (2) d_b, the thickness of an underlying layer of bulk density; and (3) f_v, the surface layer bond-packing density, expressed in terms of a void volume fraction. The surface layer simulates either the nuclei in the earliest stages of growth or the residual surface roughness layer after the nuclei make contact to form the first bulk density monolayer.

Figure 23 shows d_s and d_b, obtained as a function of time during the growth of a-Si:H onto c-Si by rf PECVD in the parallel-plate configuration. Conditions were set for optimum material: 250°C substrate temperature, 0.2 Torr pressure, and 2 W rf power (52 mW/cm^2 at sample). When the plasma is struck, the bulk layer remains near 0 Å in thickness, but the surface layer (simulating the initial nuclei) grows rapidly. The growth rate of the nuclei begins to saturate near t=10 s as nuclei make contact. The first bulk monolayer (d_b=2.5 Å) is formed at $t=t_b$=13 s, and at this point, a surface roughness layer 19.5 Å thick remains from the initial nucleation process. The most interesting aspect of the growth process is the evolution of this surface layer in the bulk film growth regime. The results of Fig. 23 show that the surface smoothens with subsequent deposition -- by about 8 Å in the first 50 Å of bulk film growth.

This behavior can be understood from continuum models of film growth [26]. In these models, the stability of one dimensional surface profiles have been studied in response to sinusoidal perturbations of spatial wavelength λ_r. Effects of finite atomic size and shadowing are proposed to enhance the perturbations, whereas adatom surface diffusion smoothens them. Basically, one expects to regain a smooth profile for $\lambda_r<\lambda_o$, the surface adatom diffusion length; however when $\lambda_r>\lambda_o$, the surface roughens, eventually stabilizing with features that appear analogous to columnar microstructure. These theories make direct contact to our experimental situation. If the nucleation-induced roughness present at time $t=t_b$ in Fig. 23 is assumed to exhibit a hemispherical geometry, then a dominant roughness wavelength of $\lambda_r \sim 2d_s(t=t_b) \sim 40$ Å is predicted. Thus, in order for this profile to smoothen, as is observed experimentally, then the precursor diffusion length must be greater than 40 Å under optimum PECVD conditions.

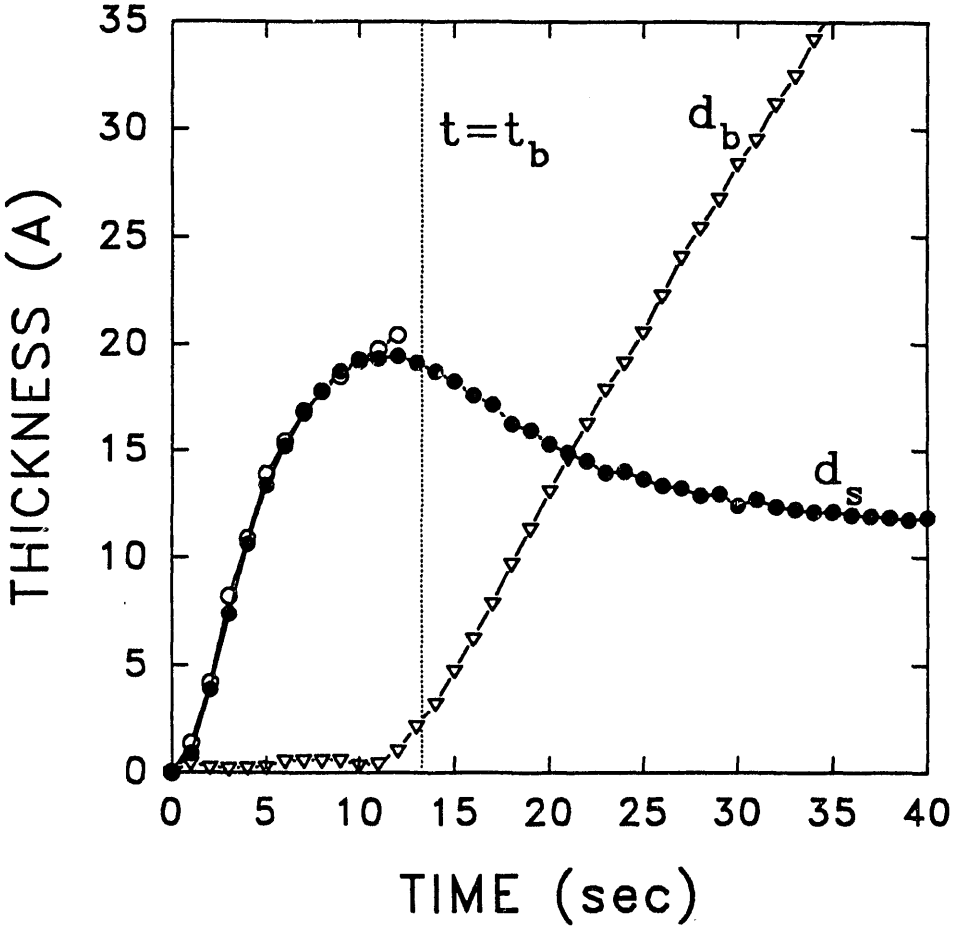

Fig. 23 Thickness of the low density surface layer representing roughness (d_s, solid points) and thickness of the bulk layer (d_b, triangles) deduced in an analysis of real time SE data collected during the nucleation and growth of optimum PECVD a-Si:H on a c-Si substrate held at 250°C. The open circles were obtained using a one-layer model for the film in the nucleation regime, where the film consists of discontinuous clusters. The decrease in d_s after the formation of the first bulk monolayer is a surface smoothening phenomena, representing coalescence of the nucleation-related clusters.

Figure 24 shows the magnitude of the smoothening effect in the first 50 Å of bulk film growth plotted vs. substrate temperature and plasma power flux at the sample surface for both remote-He and parallel-plate a-Si:H PECVD. In most cases the substrate was c-Si. It is noteworthy that the films prepared under conditions known to be optimum for parallel-plate rf PECVD, i.e. low power and T_s~250°C, exhibit the greatest smoothening effect. The clear trends to weaker surface relaxation at higher power and both higher and lower T_s, appear to reflect trends in precursor surface diffusion length. Specifically, as the diffusion length decreases the Fourier components in the surface roughness with $\lambda_T > \lambda_0$ tend to stabilize, leading to the weaker relaxation effect. The lower λ_0 for T_s<250°C arises from a thermally-assisted diffusion process. The lower λ_0 for T_s>250°C probably arises because the H-coverage of the surface is reduced, and this provides reactive sites for precursor attachment. The effect of high power is more complex. With a greater ionic flux, an effect similar to that at high T_s is possible, i.e. a greater number of sites for surface bonding. Alternatively a higher concentration of SiH and SiH_2 may be generated in the plasma, and these are more reactive at the surface [2]. In either case, λ_0 is expected to decrease. Thus, we are able to characterize process-property relationships on the monolayer-scale and highlight the important role that precursor surface diffusion play in the ultimate properties of the material. Further discussion can be found in a recent publication [27].

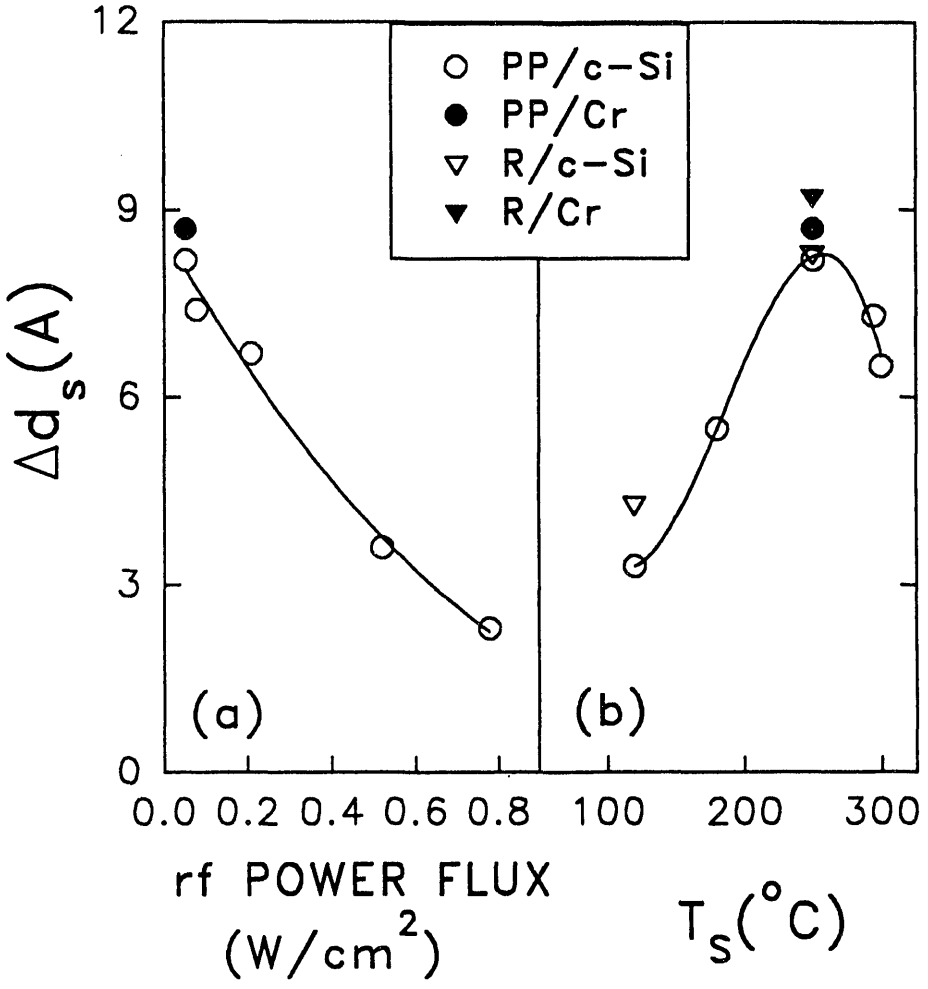

Fig. 24 The magnitude of surface smoothening, Δd_s, observed in the first 50 Å of bulk film growth for PECVD a-Si:H plotted vs. (a) rf plasma power at the substrate surface with a fixed substrate temperature of 250°C and (b) substrate temperature with a fixed plasma power flux of 52 mW/cm^2. The key is as follows PP: parallel-plate PECVD; R: remote He PECVD; Cr: Cr substrate; c-Si: Si wafer substrate. The solid lines are guides to the eye for the PP/c-Si depositions. The largest surface smoothening effect occurs for T_s~250°C and rf power < 100 mW/cm^2. The SiH_4 flow rate used in these experiments was 20 standard cm^3/min.

REFERENCES

1. K. Winer, Phys. Rev. B 41, 7952 (1990).
2. A. Gallagher and J. Scott, Solar Cells 21, 147 (1987).
3. See, for example, B.L. Stafford and E. Sabisky eds. Stability of Amorphous Silicon Alloy Materials and Devices, AIP Conf. Proc. No. 157 (AIP, New York, 1987).
4. D.L. Staebler and C.R. Wronski, Appl. Phys. Lett. 31, 292 (1977).
5. S. Zafar and E.A. Schiff, Phys. Rev. Lett. 66, 1493 (1991).
6. S.B. Zhang, W.B. Jackson, and D.J. Chadi, Phys. Rev. Lett. 65, 2572 (1990).
7. H. Shirai, D. Das, J. Hanna, and I. Shimizu, Technical Digest of International PVSEC-5 (Kyoto, Japan, 1990) p. 59.
8. R.A. Street, Phys. Rev. B 43, 2454 (1991).
9. J. Kakalios and W.B. Jackson in Amorphous Silicon and Related Materials, edited by H. Fritzsche (World Scientific, Singapore, 1988) p. 207.
10. R.W. Collins in Amorphous Silicon and Related Materials, edited by H. Fritzsche (World Scientific, Singapore, 1988) p. 1003.
11. I. An and R.W. Collins, Rev. Sci. Instrum. 62, 1904 (1991).
12. N.V. Nguyen, B. Pudliner, I. An, and R.W. Collins, J. Opt. Soc. Am. A 8, 919 (1991).
13. N. Amer and W.B. Jackson, in Semiconductors and Semimetals, Vol. 21, Part B, edited by J.I. Pankove (Academic, Orlando, FL, 1984) p. 83.
14. I. An, Y.M. Li, C.R. Wronski, and R.W. Collins, Appl. Phys. Lett. 59, 2543 (1991).
15. A.R. Forouhi and I. Bloomer, Phys. Rev. B 34, 7018 (1986).
16. K. Mui and F.W. Smith, Phys. Rev. B 38, 10623 (1988).
17. R.A. Street, C.C. Tsai, J. Kakalios, and W.B. Jackson, Philos Mag B 56, 305 (1987).
18. H.M. Branz, S.E. Asher, and B.P. Nelson, submitted for publication, 1992.
19. W.B. Jackson and C.C. Tsai, Phys. Rev. B 15, 45 6564 (1992).
20. A. Asano, Appl. Phys. Lett. 56, 53 (1990).
21. N. Maley, A. Myers, M. Pinarbasi, D. Leet, J.R. Abelson, and J.A. Thornton, J. Vac. Sci. Technol. A 7, 1267 (1989).
22. W.B. Jackson and J. Kakalios in Amorphous Silicon and Related Materials, edited by H. Fritzsche (World Scientific, Singapore, 1988) p. 247.
23. D. Das, H. Shirai, J. Hanna, and I. Shimizu, Jpn. J. Appl. Phys. 30, L239 (1991).
24. N.M. Johnson, C.E. Nebel, P.V. Santos, W.B. Jackson, R.A. Street, K.S. Stevens, and J. Walker, Appl. Phys. Lett. 59, 1443 (1991).
25. I. An, H. Nguyen, N. Nguyen, and R.W. Collins, Phys. Rev. Lett. 65, 2274 (1990).
26. A. Mazor, D.J. Srolovitz, P.S. Hagan, and B. Bukiet, Phys. Rev. Lett. 60, 424 (1988).
27. Y.M. Li, I. An, H.V. Nguyen, C.R. Wronski, and R.W. Collins, Phys. Rev. Lett. 68, 2814 (1992).

Document Control Page	1. NREL Report No. NREL/TP-451-5265	2. NTIS Accession No. DE93000051	3. Recipient's Accession No.

4. Title and Subtitle

In-Situ Characterization of Growth and Interfaces in a-Si:H Devices

5. Publication Date
December 1992

6.

7. Author(s)
R.W. Collins, C.R. Wronski, I. An, Y. Li

8. Performing Organization Rept. No.

9. Performing Organization Name and Address
Materials Research Laboratory
Pennsylvania State University
University Park, Pennsylvania 16802

10. Project/Task/Work Unit No.
PV341101

11. Contract (C) or Grant (G) No.

(C) XG-1-10063-10

(G)

12. Sponsoring Organization Name and Address
National Renewable Energy Laboratory
1617 Cole Blvd.
Golden, CO 80401-3393

13. Type of Report & Period Covered

Technical Report
1 May 1991 - 30 April 1992

14.

15. Supplementary Notes
NREL technical monitor: B. von Roedern

16. Abstract (Limit: 200 words)

This report describes the in-situ characterization of growth and interfaces in amorphous silicon (a-Si:H) devices. The growth of a-Si:H by plasma-enhanced chemical vapor deposition (PECVD) is complex and involves many gas-phase and solid-surface chemical and physical processes, which are influenced by charged particle bombardment, ultraviolet light exposure, etc. The research consisted of two broad components. The first involved preparing a-Si:H by "optimum" PECVD and exposing the film to atomic hydrogen in-situ at the growth temperature. The processes of H-diffusion and incorporation in the exposed film were studied by spectroscopic ellipsometry, giving a picture of the processes by which the chemical potential in the film equilibrates with that in the gas phase. The properties of thin films were then prepared by alternating "optimum" PECVD growth and hydrogen exposure. Film properties were then studied again. The second component of the research is discussed only briefly in this report, as it is an outgrowth of previous work on single-wavelength ellipsometry. With the new spectroscopic capability developed at Penn State, it is now possible to quantify the nucleation and growth process of a-Si:H films

17. Document Analysis

a. Descriptors
characterization ; growth ; interfaces ; amorphous silicon ; devices ; photovoltaics ; solar cells

b. Identifiers/Open-Ended Terms

c. UC Categories
271

18. Availability Statement
National Technical Information Service
U.S. Department of Commerce
5285 Port Royal Road
Springfield, VA 22161

19. No. of Pages
60

20. Price
A04

Form No. 0069E (6-30-87)

END

DATE
FILMED
3/4/93